Palaeoproterozoic reworking of Early Archaean lithospheric blocks: rocks and zircon records from charnockitoids in Volgo-Uralia

Svetlana V. Bogdanova[a,†], Elena Belousova[b], Bert De Waele[c], Alexander N. Larionov[d], Sandra Piazolo[b,e], Alexander V. Postnikov[f], Alexander V. Samsonov[g]

[a]*Department of Geology, Lund University, Lund, Sweden, svetlana.bogdanova@geol.lu.se*

[b]*ARC Centre of Excellence for Core to Crust Fluid Systems/GEMOC, Department of Earth and Environmental Sciences, Macquarie University, NSW 2109, Australia, elena.belousova@mq.edu.au*

[c]*Fortescue Metals Group Limited, Perth, Australia, bdewaele@fmgl.com.au*

[d]*Centre for Isotope Research, Karpinsky Russian Geological Research Institute (CIR VSEGEI), Saint-Petersburg, Russia, alexander_larionov@vsegei.ru*

[e]*School of Earth and Environment, University of Leeds, UK, s.piazolo@leeds.ac.uk*

[f]*Department of Lithology, Gubkin State University of Oil and Gas, Moscow, Russia, postnikov.a@gubkin.ru*

[g]*Institute of Geology of Ore Deposits, Petrography, Mineralogy and Geochemistry (IGEM) RAS, Moscow, Russia, samsonovigem@mail.ru*

Corresponding author. Tel.: +7 903 5246750;E-mail address: samsonovigem@mail.ru (Alexander Samsonov).

Keywords: Volgo-Uralia, Palaeoarchaean crust, enderbites, charnockites, tonalites

Abstract

The Volgo-Uralia segment, which constitutes one fourth of the East European Craton, is covered by sedimentary deposits. From geophysical studies and examination of thousands of drillcores, Volgo-Uralia has been recognised as a vast high-grade terrain with a complex crustal history extending from the Palaeoarchaean to the Palaeoproterozoic. Our recent studies are focused on the search for the oldest crust formation event by extracting whole rock Sm-Nd and zircon U-Th-Pb and Lu-Hf isotope information from samples recovered by drilling in southern Volgo-Uralia. Particular attention is devoted to the Kolyvan charnockitoid rock suite, which makes up several large areas of gneisses and granitoids of enderbite, charnockite and tonalite composition.

The zircon from the granitoids show complex internal structures and consists of large magmatic cores with oscillatory zoning, surrounded by CL black-and-bright bands of metamorphic rims. The crystallisation age of the cores is defined as 3140 ± 7 Ma (SHRIMP) and 3127 ± 46 Ma (LA-ICPMS), while the CL-bright rims are dated at 1950 ± 25 Ma (LA-ICPMS). The ingressive recrystallisation of primary magmatic zircon correlates with depletion in REE, which is observed in each studied core-rim pair. No differences in O-isotopic compositions have been detected between the cores and the rims. δO^{18} values with an average of 5.8 ± 0.3‰ (1SD) implying that no supracrustal rocks were involved in the source of the Kolyvan melts. The Hf-isotope compositions of magmatic cores (-3 to -9 $\varepsilon_{Hf}T$) and metamorphic rims (-14 to -28 $\varepsilon_{Hf}T$), and their similar crustal model ages from 3.42 to 3.86 Ga indicate Eo- to Palaeoarchaean crustal sources for the charnockitic magmas. Sm-Nd model ages of ca 3.46 Ga for the Kolyvan rocks are consistent with the zircon Hf-isotope data and indicate a long crustal prehistory of a source of the Mesoarchaean magmas.

We conclude that the Mesoarchaean Kolyvan suite rocks was formed by reworking of Eo- to Palaeoarchaean lithosphere, which probably had been widespread throughout Volgo-Uralia. The obtained geochemical and isotope data can be reconciled in a model of deep mantle-plume activity at 3.1 Ga causing mantle underplating, extension of the Palaeoarchaean crust and high-T magmatism.

1. Introduction

It is widely recognised that Archaean lithospheric blocks are the building stones of Precambrian cratons. The extremely depleted subcontinental lithospheric mantle (SCLM) provided their buoyancy and stability (Griffin et al., 2014; Griffin et al., 2003). Being the cores of continents, Archaean blocks played a crucial role in the formation and breakup of supercontinents defining plate motions and their reorganisation during supercontinental cycles (Artemieva and Mooney, 2002; Brown, 2008; Condie et al., 2015; Condie and Kröner, 2008; King, 2005). However, our knowledge of the global distribution and sizes of the Archaean blocks is constrained by their limited exposure of an estimated 20 % of the overall craton areas (Goodwin, 1991), while their major parts are overlain by thick platform covers or fragmented within younger orogenic belts. The crystalline crust of Volgo-Uralia, one the major lithospheric segments of the East European Craton, is hidden completely beneath an up to 20 km thick sedimentary cover. Multiple hydrocarbon prospecting drillholes have penetrated up to 4 km thick platform cover allowing to sample basement rocks (Muslimov and Lapinskaya, 1996). From geophysical studies and the examination of drill cores, the crystalline crust of Volgo-Uralia has long been recognised as a high-grade terrain with a crustal history extending from the Archaean to the Palaeoproterozoic (Bogdanova, 1986; Bogdanova et al., 2010; Bogdanova et al., 1978; Postnikov, 2002). Archaean high-amphibolite- to granulite facies rocks make up about 70 % of its territory, amongst which intrusive charnockitoids (enderbites and charnockites *s.s.*) and orthopyroxene-plagioclase gneisses account for 25-30 %.

Charnockitoids are rocks indicative of high-grade metamorphic terrains. Being high-temperature granitoids, they relate to the specific P-T-fluid regimes and geodynamics of crust formation e.g. (Rajesh and Santosh, 2012). The wide distribution of these high-temperature igneous rocks in the Archaean crust of Volgo-Uralia raises the important question as to what kind of tectonic setting allows such high temperature magmatism to take place. The current discussions are mostly centered on a plate tectonic or a mantle plume explanation (Bédard, 2018; Gerya, 2014; Gerya et al., 2015; Moyen and Laurent, 2018; Sizova et al., 2015).

The idea that the crust and corresponding lithospheric mantle in Volgo-Uralia can be Palaeoarchaean was confirmed for a granitoid block in its central part (Bogdanova et al., 2010). In the present study, we revisit the Kolyvan charnockitoids in south-western Volgo-Uralia (Fig. 1) to elucidate its origin and age, trace-element chemistry and the Hf- and O -isotopic characteristics of the zircon hosted by the magmatic enderbites and related granitoids. We supplement chemical analyses with a microstructural investigation linking the complex CL zircon structure and the internal changes in crystallographic orientation of the zircon cores and rims using electron backscatter diffraction (EBSD) techniques to investigate the possible imprint of metamorphism and deformation.

2. The geological framework of Volgo-Uralia and its charnockitoids

Volgo-Uralia is constituted of several Neoarchaean (2.8-2.7 Ga) crustal blocks separated by extensive deformational belts formed between 2.10 and 1.95 Ga (Fig. 1, inset). The largest orogenic belt is the 2.1-2.0 Ga Volgo-Don Orogen along its southwestern margin, interpreted to be a collisional belt comprised of thrust sheets extending over the Archaean autochthon

(Mints, 2011)(Bogdanova et al., 2012; Savko et al., 2015). Along the NW margin of Volgo-Uralia, the accretionary Osnitsk-Mikashevichi-Moscow magmatic belt developed 2.00-1.95 Ga ago (Bogdanova et al., 2006). Ar-Ar and K-Ar dating of amphibole and biotite (Bogdanova, 1993; Lobach-Zhuchenko et al., 1979; Polevaya, 1978; Postnikov, 1976) indicate that the present architecture of Volgo-Uralia was shaped between 1.9 and 1.7 Ga.

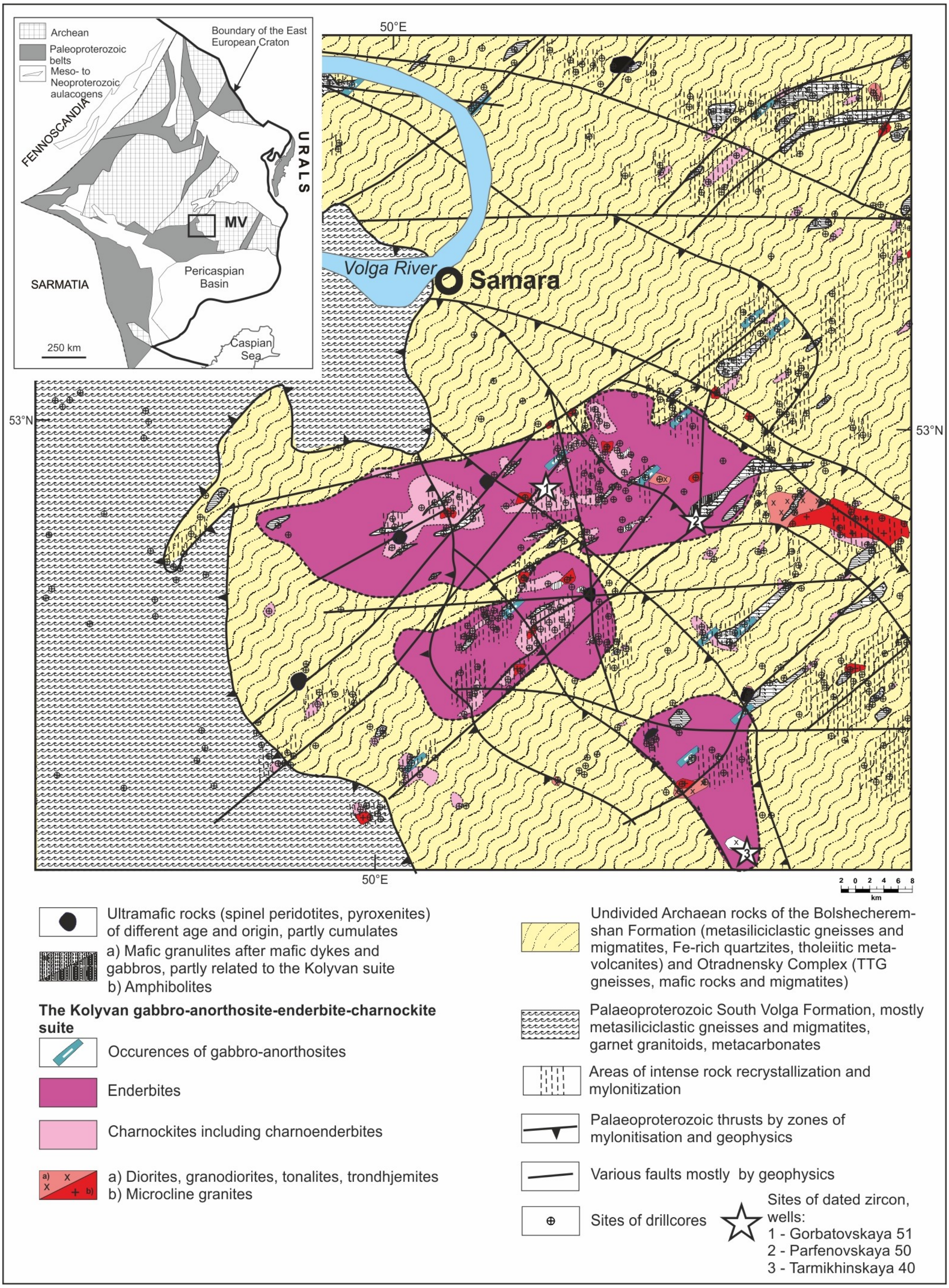

Fig. 1. The map of the Samara region in southern Volgo-Uralia showing the setting of the Kolyvan gabbro-anorthosite-enderbite-charnockite suites. The most important features are: 1. The Kolyvan intrusions are separated by the complicated fault system related to the Volgo-Sarmatian collision; 2.

the intrusive charnockites are intensively recrystallised and mylonitised along faults and thrusts. 3. Enderbites and charnockites s.s. characterise two major phases of crustal melting. The inset presents the major tectonic subdivisions of Volgo-Uralia (Bogdanova et al., 2016) (MV – the Middle Volga megablock)

The crust of the Middle Volga megablock in central and southern Volgo-Uralia (Fig. 1, inset) is made up of alternating supracrustal and meta-igneous belts reflecting a complex fold-and-fault structure of the crust as revealed by magnetic anomalies and seismic profiling (Bogdanova et al., 2016; Trofimov, 2006). This structure was formed during the Neoarchaean collision at 2.73-2.65 Ga, but then strongly reworked at ca. 2.00-1.95 Ga. Charnockitoids (charnockites *s.l.*) are widespread throughout the igneous belts (Bogdanova, 1986; Muslimov and Lapinskaya, 1996). They have long been thought to be mostly Neoarchaean based on a few U-Pb zircon ages of 2738 ± 12, 2725 ± 42 and 2709 ± 16 Ma (Bibikova et al., 1984; Bibikova et al., 1994). However, our preliminary results (Bogdanova et al., 2013) suggest that sizeable parts of the crust in the Middle Volga megablock comprise charnockitoids of Palaeo- and Mesoarchaean ancestry.

It is widely accepted that charnockitoids belong to two genetic groups, one representing crystallisation of anhydrous silicic magmas and the other created by metamorphic dehydration of biotite-amphibole bearing granitoids or orthogneisses (Rajesh and Santosh, 2012). However, Frost and Frost (2008) proposed that only the magmatic group should be named “charnockites”. The charnockitoids in Volgo-Uralia are mostly magmatic and comprised of gabbro-(anorthosite)-enderbite-charnockite (GEC) suites, which possibly make up large intrusions. When subjected to high-grade metamorphism and deformation, the GEC rocks turn into orthopyroxene-bearing gneisses and high-grade mylonites. Metamorphic rocks may also have formed by granulite facies metamorphism, melting and migmatisation of supracrustal rocks.

These occur as small bodies and veins with enderbitic or charnockitic compositions (Bogdanova, 1986).

3. Methods

Analytical work for this study was conducted in several laboratories around the world using various analytical methods over several years of collaboration. Whole-rock major analyses were carried out on fused glass discs using a PW-2400 X-ray sequential fluorescence spectrometer at Institute of Geology of Ore Deposits, Petrography, Mineralogy and Geochemistry at the Russian Academy of Sciences (IGEM RAS), Moscow, Russia . Some major and all whole-rock trace-element analyses were performed by ICP-ES and ICP-MS techniques at the ACME Analytical Laboratories in Vancouver. Whole-rock Nd-isotope data were obtained using conventional method at the isotope laboratory of the Vernadsky Institute of Geochemistry and Analytical Chemistry RAS in Moscow. Thin sections of the rock samples and zircon grain mounts were studied under a Tescan Mira3 High Resolution Schottky FEG-SEM instrument at the laboratory of the Department of Geology in Lund University, Sweden. The electron backscatter diffraction (*EBSD*) analyses on zircon were carried out on the Carl Zeiss IVO Scanning Electron Microscope (SEM) of Macquarie GeoAnalytical (Macquarie University, Australia). Zircon U-Pb age data were collected using SHRIMP instruments at the VSEGEI (St Petersburg) and Curtin (Perth, Australia) laboratories, while LA-ICPMS method was used at Macquarie GeoAnalytical. In-situ U-Pb dating and trace-element analysis on zircon were conducted using the Agilent 7700 quadrupole ICP-MS and Hf-isotope analysis using Nu Plasma multi-collector ICPMS instruments at the Macquarie GeoAnalytical laboratories. A Cameca IMS 1280 multi-collector ion microprobe located at the Centre for Microscopy, Characterisation and Analysis (CMCA) of the University of Western Australia was used for the zircon O-isotope analyses. More details on the individual analytical methods used are provided in Appendix 1.

4. The Kolyvan charnockitoid rock suite

4.1 Geology of the Kolyvan charnockitoids

The Kolyvan charnockitoid rock suite (KCRS) covers several large (up to 1300 km^2) areas of coarse- to medium-grained magmatic charnockitoids that have been recovered by drilling in southern Volgo-Uralia. It extends for 65 km by 20 km with two smaller satellite bodies in the south, which are possible parts of the KCRS displaced along fault zones (Fig. 1). The KCRS mostly comprises enderbites and is outlined by low-to medium intensity magnetic anomalies that correspond to variable magnetic susceptibilities of rocks reaching $3320*10^{-6}$ SGS units (Bogdanova, 1986). In numerous drillcores, the enderbites are accompanied by leucogabbro and gabbro-anorthosites. Small bodies of charno-enderbites and charnockites may represent late surges of residual melts. Some varieties of the Kolyvan rocks are amphibole-biotite bearing granitoids containing antiperthitic plagioclase and rare hypersthene. Within the KCRS, several wells have revealed single ultramafic rock occurrences that could represent mantle xenoliths within KCRS.

The host rocks of the Kolyvan pluton are difficult to identify because of the absence of direct wallrock contacts in the available drillcores. However, it is likely to be the high-grade aluminous metasedimentary gneisses identified outside the KCRS, although Late Archaean and Palaeoproterozoic rocks can also be tectonically interleaved with the charnockitoids (Bibikova et al., 2015; Bibikova et al., 2009).

The KCRS was intruded by mafic dykes (*not dated*), and then experienced high amphibolite-to-granulite metamorphism and deformation during the Volgo-Sarmatian collision at ca. 2.1-2.0 Ga and later (Bogdanova et al., 2008; Bogdanova et al., 2012). The zones of most intense metamorphism and deformation predominantly trend NNW-SSE and track the tectonic structural orientation of the adjacent Palaeoproterozoic Volgo-Don collisional orogen with its numerous faults (Fig. 1). Mylonites at high-grade amphibolite facies metamorphism and, at least in part, with evidence of migmatisation, occupy wide areas delineating fault zones. The 2.1-2.0 Ga tectonic fabric was overprinted by NE-NNE faulting and deformation between 2.00 and 1.95 Ga, typical for most of the Middle Volga megablock.

3.2 Petrography and chemical composition of the Kolyvan rock suite

The Kolyvan charnockitoids are coarse- to medium grained rocks (Figs. 2 and 3) and made up of antiperthitic plagioclase (An 30-54), perthitic orthoclase, quartz, hypersthene (#Mg 0.50-0.60), amphibole and biotite in variable proportions. Apatite, zircon and Ti-magnetite are abundant accessories.

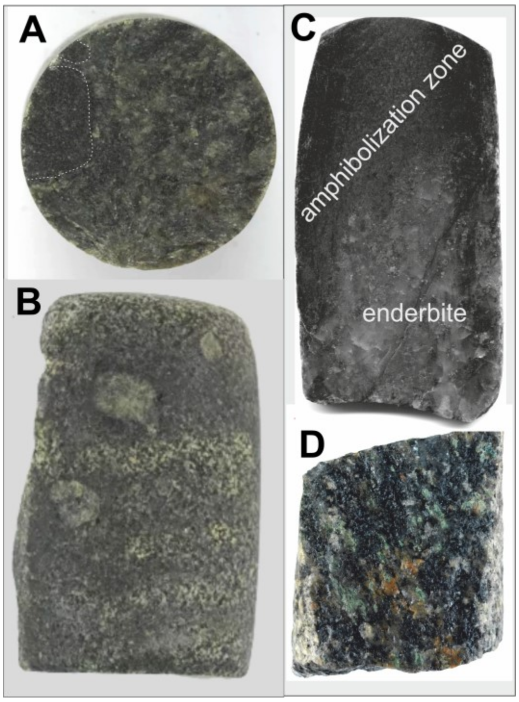

Fig. 2. Description of rocks of the Kolyvan suite. A - a coarse-grained enderbite, bearing enclaves of fine-grained gabbro-norites outlined by the white dashed line (the Kolyvan 81 drillcore, depth 2414 m). B - euhedral plagioclase inclusions in medium-grained gabbro-norites indicating probable mingling (the same drillcore). C - a zone of strong amphibolisation of the coarse, slightly deformed enderbite (the same drillcore). D - the granodiorite from the Tarmikhinskaya 40 drillcore, depth 3750 m. The drillcore diameters are 5 cm.

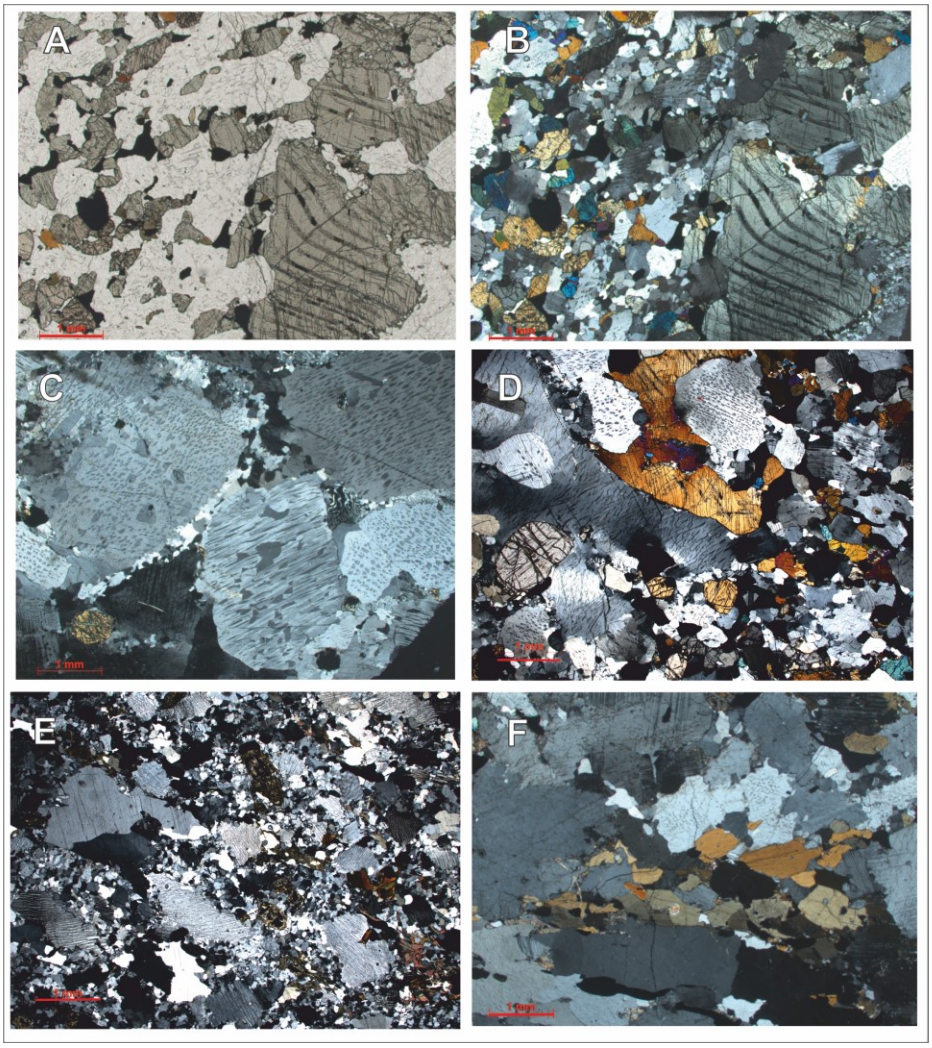

Fig. 3. Representative microphotographs of the Kolyvan rocks.

A (plane polars) and B (crossed polars) show strongly deformed gabbro-anorthosite with large exsolved igneous orthopyroxene lamellae, surrounded by fine-grained metamorphic aggregates of orthopyroxene, clinopyroxene, andesine and quartz. When compared, "A" reveals proto-igneous plagioclase grains, replaced by fine-grained metamorphic assemblage of feldspars and quartz; C and D (crossed polars) represent the typical well-preserved enderbites of the Kolyvan suite dated in this *study. (C). Coarse antiperthitic plagioclase is recrystallised along its boundary where small euhedral plagioclase with quartz, amphibole and biotite form clusters of anatectic tonalites (D). Myrmekites are interstitial to feldspars; E (crossed polars): strongly deformed charnockite of the Kol 2 suite. Microperthitic K-feldspar is elongated and aligned with mylonitic foliation. Fine-grained matrix has polygonal microstructure in some places indicating solid-state annealing after deformation; F: An amphibole-biotite-bearing tonalite-enderbite*

In the enderbites, subhedral plagioclase is outlined by aggregates of orthopyroxene and Ti-magnetite, in part replaced by brownish amphibole and biotite. Coarse-grained hypersthene exhibits exsolution structure (Fig. 3 A and B). Most of the rocks, however, have been deformed and recrystallised to various degrees, where rocks with the highest degree of deformation represent high-grade protomylonites (Fig. 3 E). Deformed, broken and displaced fragments of magmatic antiperthite, microperthite and orthopyroxene are set in a matrix consisting of fine-grained, commonly polygonal metamorphic diopside, plagioclase and quartz ± amphibole, biotite and K-feldspar, which envelopes the magmatic minerals (Fig. 3). In places where H_2O-rich fluids were present, fine-grained amphibole-biotite-plagioclase-quartz aggregates developed along these fine grained, recrystallised deformation zones (Fig. 3 F).

The granitoids, varying from granodiorites to tonalities, are coarse- to medium-grained rocks composed of amphibole, biotite, plagioclase, including antiperthite, and quartz (Figs. 2 and 3). Zircon, apatite and Ti-magnetite are accessory minerals. Deformed varieties are characterised by fine-grained zones of recrystallisation with high amounts of quartz.

Since the original magmatic minerals of the Kolyvan rocks were partly replaced by metamorphic minerals, it is problematic to classify the rocks by their modal compositions. Also, they are often coarse-grained, which makes it difficult to assess the mineral proportions. Based on their chemistry (Table 1 and Appendix 2) and normative compositions, the Kolyvan rocks in the main pluton ("Kolyvan 1" or "Kol 1" suite hereafter) range from gabbro-anorthosite, monzodiorite (mangerites) to tonalite/enderbite (Fig. 4). Charno-enderbites and charnockites (the "Kolyvan 2" or "Kol 2" suite), which form separate small bodies within the enderbites (Fig. 1), plot along a different, tonalite-granite trend both in QAP and An-Ab-Or diagrams (Fig. 4). Some deviations from these trends may be due to transitional rock compositions.

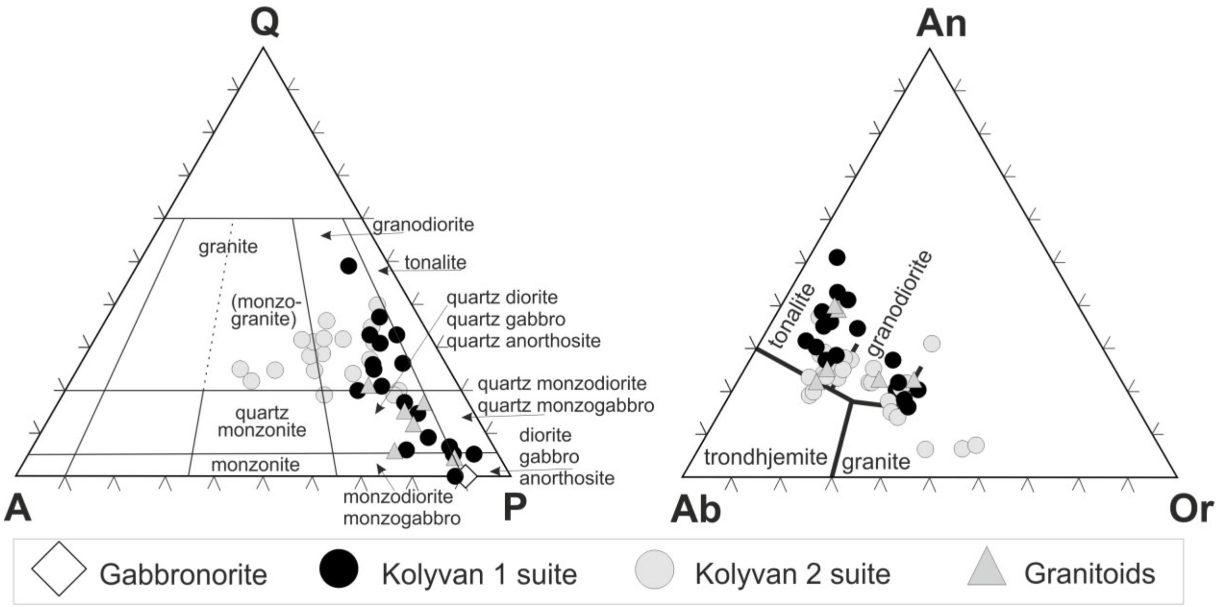

Fig. 4. QAP and An-Ab-Or normative classification of the Kolyvan charnockitoids. QAP rock subdivisions are according to Le Maitre (2002) and An-Ab-Or to Baker (1979).

When using the chemical classification of Frost et al. (2001) for granitoids, both Kolyvan suites range between ferroan and magnesian, medium- to high K, mostly peraluminous, and belong to the calc-alkalic and calcic series (Fig. 5). Despite some deviations, the variations of the major elements (Fig. 6) follow near-continuous trends for both the Kol 1 and Kol 2 suites indicating their comagmatic origin.

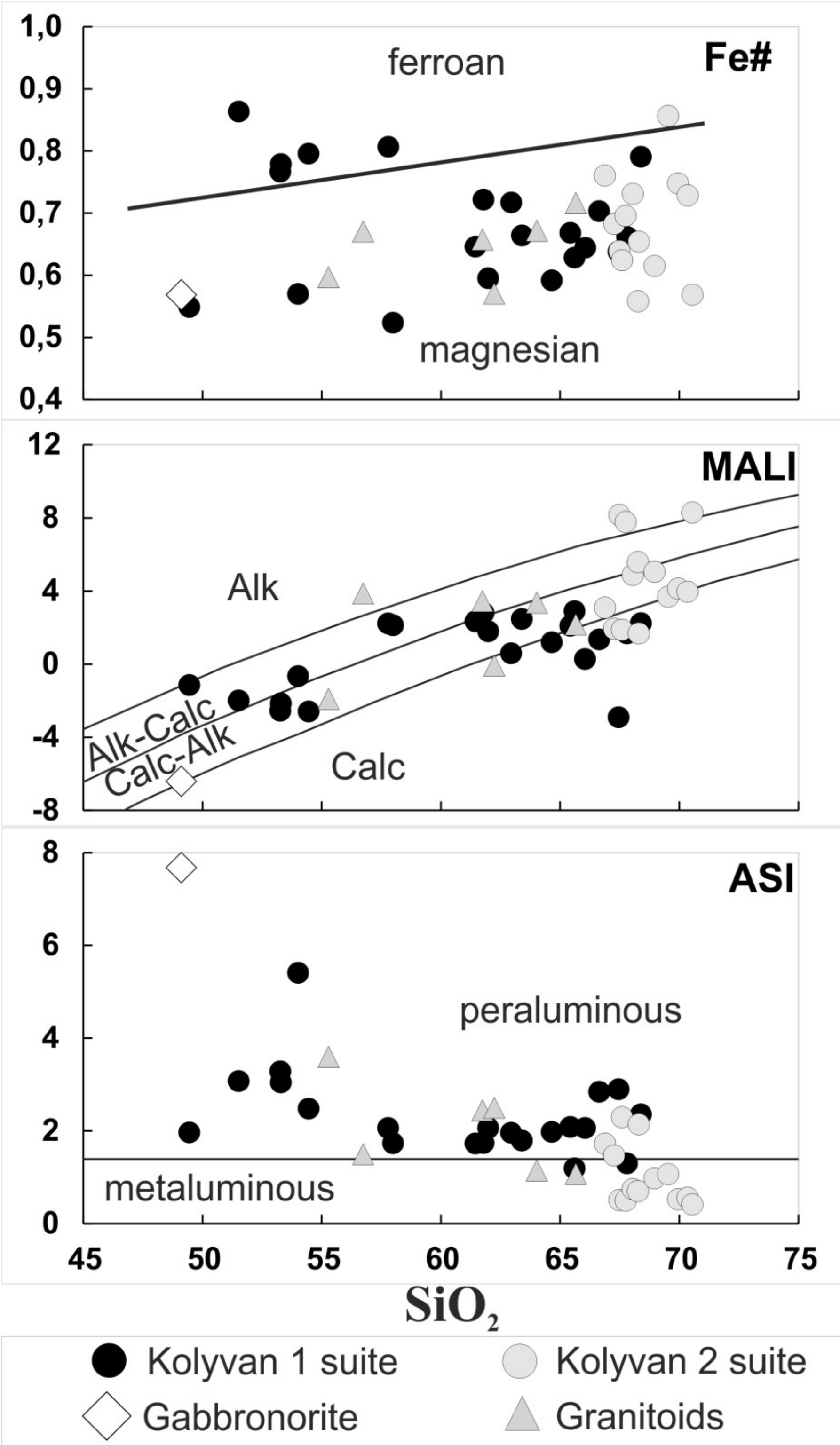

250

251 *Fig. 5. The Kolyvan rocks according to granitoid classifications by Frost et al. (2001).*

252

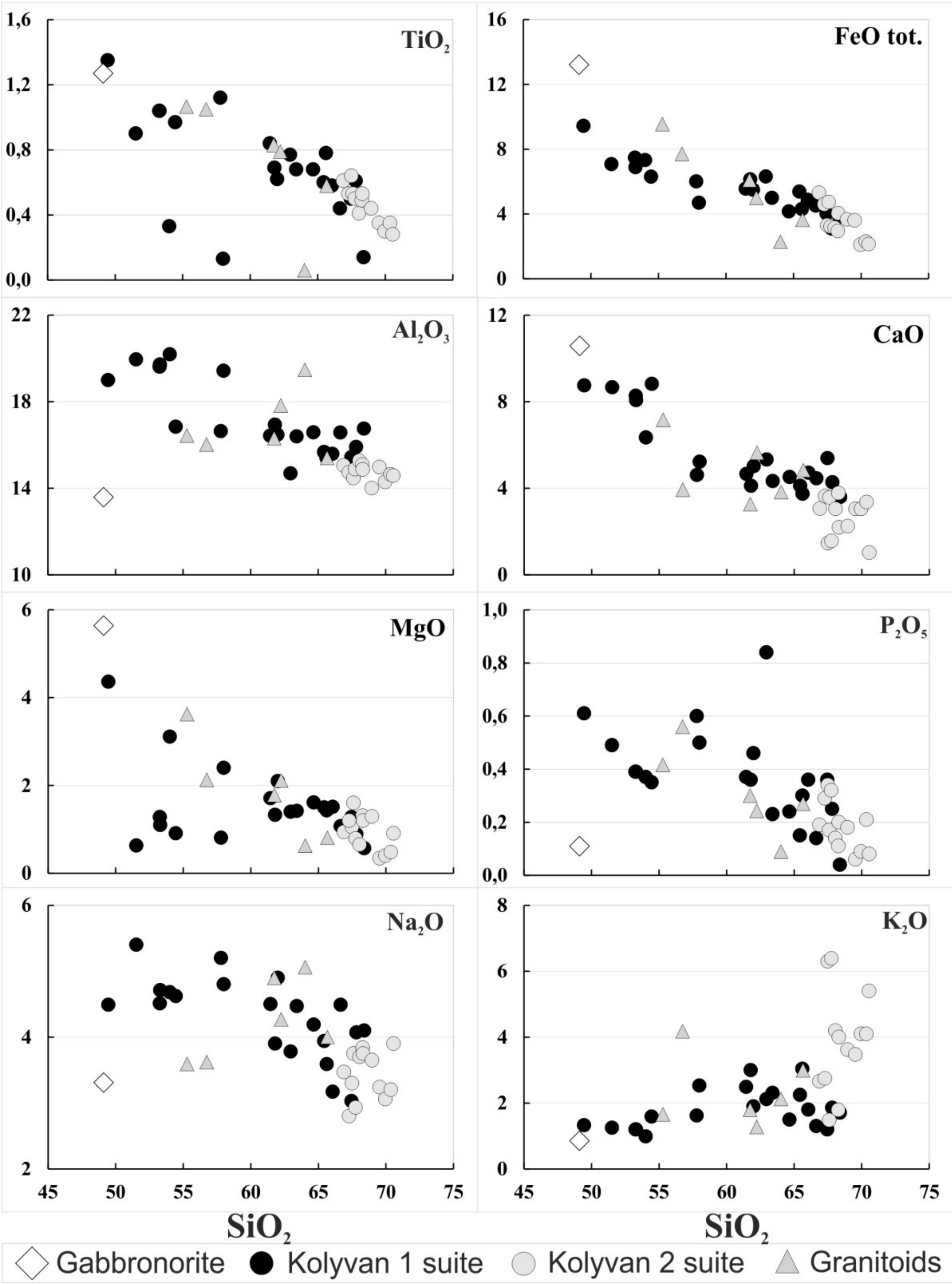

Fig. 6. Variations of the major elements in the Kolyvan rocks against SiO_2 contents.

Among the Kol 1 rocks, two groups can be recognised (Fig. 6). The first group has SiO_2 contents varying from 49.5 to 54.5 %, and shows higher contents of TiO_2, FeO, high Al_2O_3 and CaO.

These rocks contain up to 70-75 % plagioclase (An 54-42) and are leucogabbros, gabbro-anorthosites and quartz anorthosites according to the QAP classification (Fig. 4). They stand out, having higher Sr contents reaching ca. 1000 ppm and higher Sr/Y ratios, Cr and Ni contents (Table 1). One gabbro-norite (sample 81-1) departs from the rest (Figs. 6 and 7) by its high MgO content, low Sr/Y and a REE smooth pattern, with a $(La/Yb)_N$ value of 7, which is about 10 times more than “Primitive Mantle“ contents.

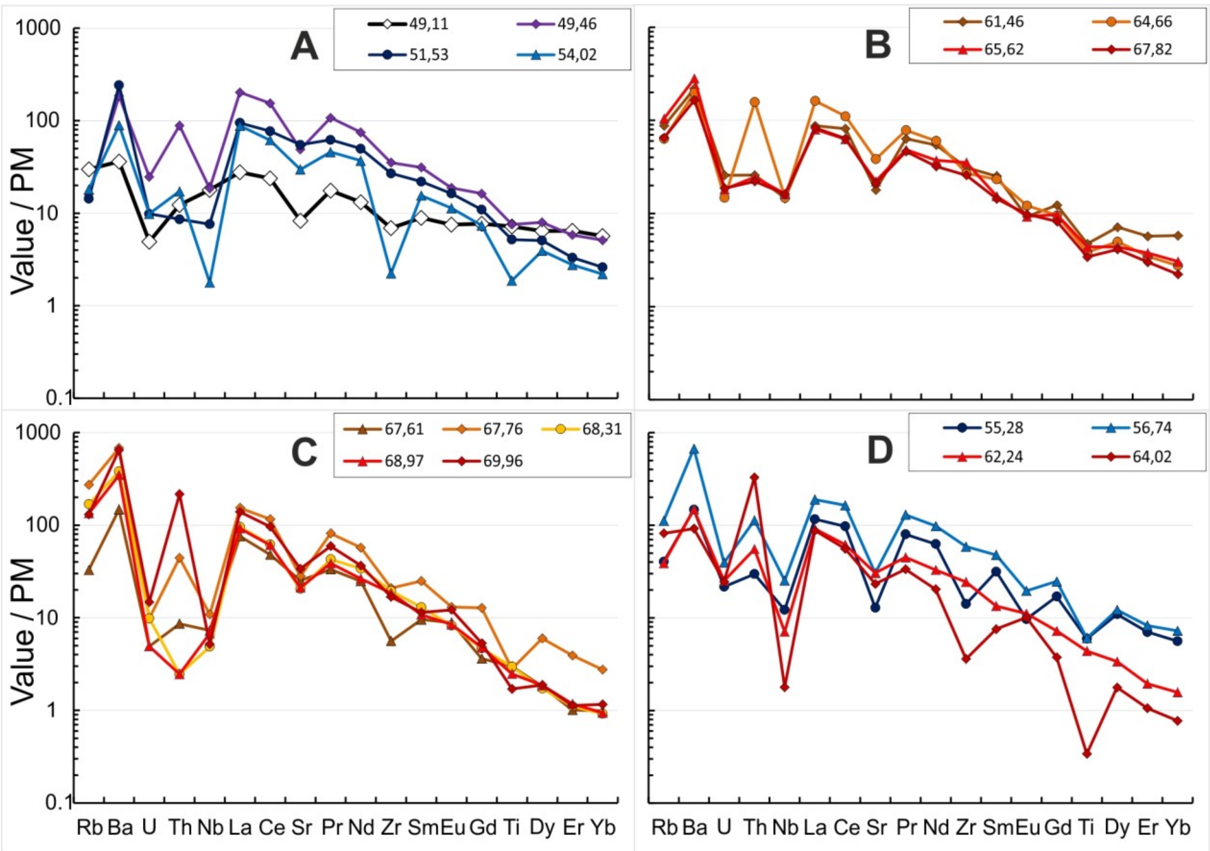

Fig. 7. Multielement diagram for Kolivan rocks: A – low-Si Kol-1 suite and gabbronorite (black line); B - high-Si Kol-1 suite; C - Kol-2 suite; D – granitoids. Values in legends – concentrations of SiO_2 in the samples

The more abundant second (enderbite *sl*) group of the Kol 1 suite plots between quartz gabbro, diorite, granodiorite and tonalite (Fig. 4) with SiO_2 contents between 57.8 and 68.4 %, and variable Al_2O_3 and MgO amounts reflecting variable contents of orthopyroxene and plagioclase. Sr/Y ranges between 12 and 30 (Fig. 8). The abundances of Hf, Zr and Th as well as LREE correlate with the contents of zircon, monazite and apatite. There is no evident difference in chemistry between the enderbites (*s.s*) and their granitoid relatives, with the exception of higher variations of trace elements, and particularly of REE, controlled by the amounts of amphibole and biotite (Fig. 7, B).

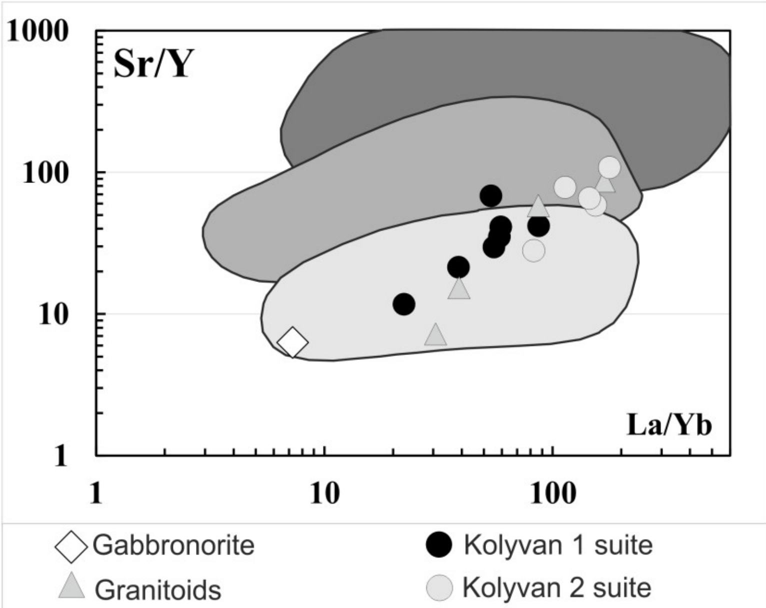

Fig. 8. Sr/Y vs La/Yb in the Kolyvan rocks indicating their melting at low- to medium pressures. The TTG fields of high pressure (darkest grey), medium pressure (medium grey) and low pressure (light grey) are modified from Moyen (2011)and Moyen and Martin (2012)

The Kol 2 suite features a more consistent evolution of the major elements which, with the exception of K_2O (Fig. 6), all decrease with increasing of SiO_2 (67 to 71 %). Different from the Kol 1 rocks, the charno-enderbites and charnockites of the Kol 2 suite have a higher total average REE (up to 240 ppm) and two times lower HREE (Fig. 7 B, Table 1).

3.3 Sm-Nd isotope features of the Kolyvan rock suite

The three analysed samples of the Kolyvan rock suite, including one enderbite and two granitoids, have very similar Sm-Nd isotopic characteristics. They have a narrow range of Sm-Nd model ages of ca 3.46 Ga and small variations in negative εNd_T values from -1.5 to -2.1 (Table 2).

4. Characteristics of zircon from the Kolyvan rocks suite

To resolve the timing of the Kolyvan magmatism and metamorphism, zircon grains have been separated from the following samples: (a) biotite-amphibole-plagioclase-bearing granitoids spatially associated with enderbites (wells Parfenovskaya 50, N52º53' E50º39', depth 3218 m and Tarmikhinskaya 40, N52º26' E50º42', depth 3750 m; Fig.1, sites 2, and 3); (b) coarse-grained slightly deformed enderbites (well Gorbatovskaya 51, N52º55' E50º20', depth 2903 m; Fig. 1, site 1.

These samples were chosen to represent largely undeformed to metamorphosed and deformed rocks of the Kolyvan rock suite. The complex zircon from the Gorbatovskaya 51 enderbite provides the opportunity to date both magmatism and metamorphism of the Kolyvan charnockitoids. Twenty seven U-Pb SIMS and 38 LA-ICPMS in-situ analyses have been conducted for zircon from the deformed Gorbatovskaya 51 enderbite and 32 U-Pb SIMS zircon analyses for the Kolyvan granitoids.

4.1 Crystal morphology and U-Pb geochronology of zircon from the Kolyvan granitoids (wells Tarmikhinskaya 40 and Parfenovskaya 50)

Zircon from the Kolyvan granitoids (sample N39-1-1 and N39-12) is faintly colored pinkish to beige, and ranges in size from 70 to 250 μm. Representative images of the studied zircons from the Kolyvan granitoids are presented in Fig. 9 (a, c) (transmitted light) and Fig. 9 (b, d) (cathodoluminescence, CL). The vast majority of the zircon is subhedral to anhedral. Yet, their bipyramidal-prismatic morphology is still recognisable. Mineral and melt inclusions are common. The grains are fractured to various degrees. In some cases, oscillatory growth zoning can be seen even in transmitted light.

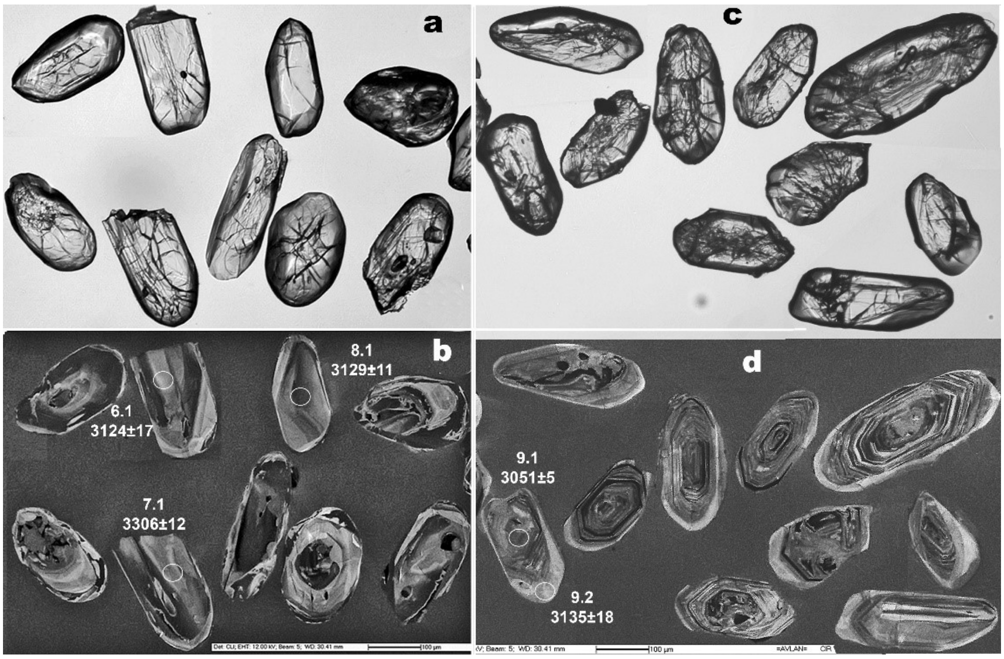

Fig. 9. Morphology and internal structure of the studied zircon from granitoids of the Kolyvan suite (wells Tarmikhinskaya 40 (N39-1-1 c, d) and Parfenovskaya 50 (N39-12 a and b). Photographs: a, c - transmitted light; b, d - cathodoluminescent. Circles depict analyses position with spot numbers (Table 8 and corresponding $^{207}Pb/^{206}Pb$ age).

The CL images demonstrate that the zircon have oscillatory concentric zoning patterns consistent with their magmatic origin. The zircon from the Tarmikhinskaya 40 sample (N39-1-1) has rather fine zoning, while the zircon from the Parfenovskaya 50 sample (N39-12) demonstrates broader-banded patterns (Fig. 9). Apart of the primary growth zoning, CL imaging reveals complex outer rims. These rims are light-grey, almost completely homogeneous (without any obvious zoning) in sample N39-1-1, while represented by CL-black and grey outgrowths in N39-12. They might have been produced as a result of a later metamorphic event and are particularly wide in sample N39-1-1. Some zircon from sample N39-12 have central domains structurally discordant to the main magmatic zircon (e.g., the fourth grain in the bottom row, Fig. 9b): those cores are most probably inherited from the precursor rock**.**

A total of 16 analyses on 9 zircon grains were carried out for the Tarmikhinskaya 40 tonalite-enderbite (sample N39-1-1) in order to date both the inner core and the outer rim on the same grain (Fig. 10 A). No considerable discrepancies in age were found between the rims and the central parts (Table 3), although rims with lower U content (as low as 91 ppm in grain #9.2), yielded more concordant results. A possible assumption is that the U-Pb systematics of the internal parts have been totally reset by the event that formed the outer rims. However, some of the analysed internal parts also have relatively low U concentrations (several hundreds of ppm), and should not be prone to a complete reset of the U-Pb system. The U-Pb data for both the internal domains and the CL-light rims are presented together on the same plot (Fig. 10 A). All the 16 results form a regression line (Fig. 10 A) with upper intercept age of 3131 ± 7 Ma (MSWD = 1.05), which is accepted as the crystallisation age of the protolith. Hence, it may be suggested that the outer rims have been formed during the same magmatic crystallisation process: similar zircon structures with late CL-bright outer rims are known, though from other rock types (e. g. Grimes et al., 2009).

For the Parfenovskaya 50 sample (N39-12) a total of 16 analyses on 10 zircons grains were conducted with two of those located within the rims, structurally discordant to the oscillatory-zoned internal domains (Fig. 10 B, analyses 1.2 and 2.2 in Table 3). One analysis on the inner part of the grain (7.1, Table 8) gave a considerably older age ($^{207}Pb/^{206}Pb$ - c. 3.3 Ga) and was interpreted as an inherited core. Two other younger apparent ages ($^{207}Pb/^{206}Pb$ - c. 3.08 Ga; 5.1

and 9.1) are attributed to Pb-loss. The rest of analyses form a compact array of near-concordant data. Notably, no considerable age difference was revealed between the internal domains and outer rims. A discordia line through those 13 points yields an upper intercept at 3137 ± 15 Ma (MSWD = 0.09), interpreted as the magmatic crystallisation age of the protolith. The observed close similarity of rims and the internal zircon parts suggest they have been formed simultaneously within analytical error for the age estimate, most probably by the same crystallisation process.

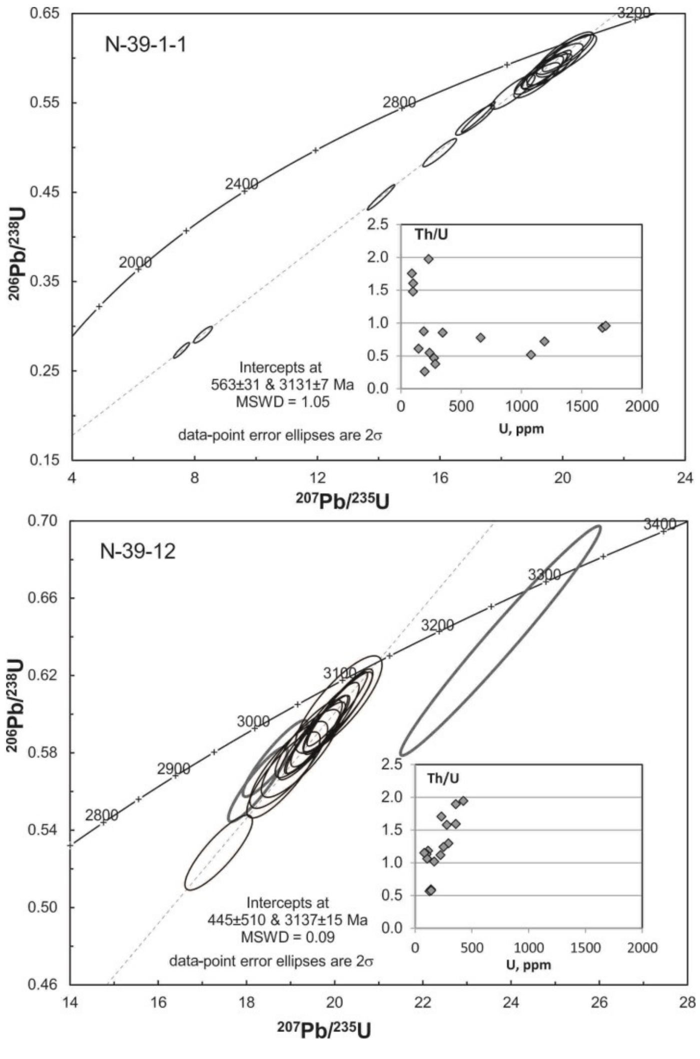

Fig. 10. Concordia diagrams for zircon from the granitoids of the Kolyvan suite. A – well Tarmikhinskaya 40, B – well Parfenovskaya 50. The lower insets show Th/U vs U contents in the dated zircon.

The overall concordance of the results in sample N39-12 is somewhat higher than that in N39-1-1. Most likely this is due to higher U and Th content in the N39-1-1 zircons with U concentrations for several grains exceeding 1000 ppm (Table 3).

4.2 Crystal morphology, U-Pb geochronology, chemical and isotope features of zircon from the Gorbatovskaya 51 enderbite

4.2.1 General morphological features

Zircon from the Gorbatovskaya 51 enderbite (sample #svt13) is pale yellow to black- yellowish in colour, and ranges in size from 100 to 400 μm. The aspect ratio varies from 1:1 to 4:1. Cathodoluminescence (CL) imaging reveals a complex internal structure of zircon with homogenous black-grey, sector and oscillatory zoned, mostly irregular cores, enveloped by low- or high-luminescent CL rims (Fig. 11 and Appendix 3). Most of the grains consist of a core surrounded first by relatively thin (up to 20-30 μm) CL-black homogenous discontinuous rims and bays, and then cut by commonly thicker (up to 80μm) CL-bright ingressive, curved overgrowths, which are responsible for the ovoid shapes of zircon grains. The cores were notably fractured and fragmented prior to their final recrystallisation as can be seen from the numerous cracks that are confined to the inner parts of the grains and not projected onto the thin outer rims.

Fig. 11. Morphology and internal structure of the studied zircon from the Gorbatovskaya 51 enderbite (N 52°55'30"/ E 50°20'28"; depth of drillcore 2896-2914 m). The upper panel shows selected zircon grains in transmitted light and their CL images are in the lower panel. Notably, some cores were fractured and fragmented prior to their final recrystallisation.

4.2.2 Details of the internal structure and characteristics of the metamorphic zircon

In view of the complex structure of zircon in the Kolyvan enderbites, and evidence for potential association with metamorphism and deformation, electron backscatter diffraction (EBSD) analysis (Appendix 3) was conducted on selected zircon grains to explore to what extent crystal plastic deformation may have influenced the chemical and geochronological data and/or if replacement reaction took place. EBSD allows full (all crystallographic axes) quantitative crystallographic characterisation of a mineral with information on the spatial variations.

Orientation changes are shown in colour coded maps (Fig. 12) with abrupt changes signifying subgrain either originating from crystal plastic deformation, growth (often epitaxial i.e. same orientation as host) or fracture related zircon block rotations and healing (Rimša et al., 2007; Tretiakova et al., 2017). Crystal plastic deformation will result in a systematic change in orientation according to the slip system activated (e.g. Piazolo et al., 2012). Replacement by fluid mediated reactions results in no systematic crystallographic changes, i.e. the spread of orientation is not related to a particular rotation axis and/or subgrain boundary orientation near perpendicular to the reaction front (e.g. Spruzeniece et al., 2017). In addition to EBSD maps, we show so-called forescatter images. In such images, changes in grey scale are caused by a combination of crystallographic orientation differences and topography. As the samples are mechano-chemically polished, the polishing fluid etches the surface slightly; consequently topographic changes can be related to slight differences in chemistry causing differential etching and/or fractures (i.e. fractures etch more easily than an intact grain).

Grain #13-3 (Fig. 12) shows a clear healed crack cutting the whole grain (shown as the white-stippled line in the CL image). The CL-bright rim has a clearly defined microstructure that is typical for fluid mediated replacement textures with subgrain boundaries perpendicular to the reaction front (i.e. CL the light-black boundary) (Spruzeniece et al., 2017). Within the CL-light grey core, slight orientation changes are seen which are bounded by internal fractures.

In grain #13-33, orientation mapping of the left grain shows that the CL dark core is distinct from its surrounding. The core shape and CL-grey oscillations are governed by the crystal morphology of the grain where the straight boundaries between core and CL-grey oscillations are consistent with 2D sections of low index planes (<111> and <100> facets) (see 3D representation of the crystal orientation of the grain). EBSD analysis shows that the core was subject to fracturing and fracture related rotations as orientation changes are distinctly blocky, with distinct lines of orientation change surrounding areas of similar orientation. The CL-black rim is not distinct, however the very outer CL-bright rim exhibits subgrain boundaries that are perpendicular to the core-rim interface suggesting that this rim was formed by replacement reaction. In the right grain (image #13-33), the dark-grey magmatic core is again clearly distinct from the CL-greyish (bright) rim, where the latter is irregular in orientation shown as the mottled blue-green EBSD signal suggesting resorption and overgrowth.

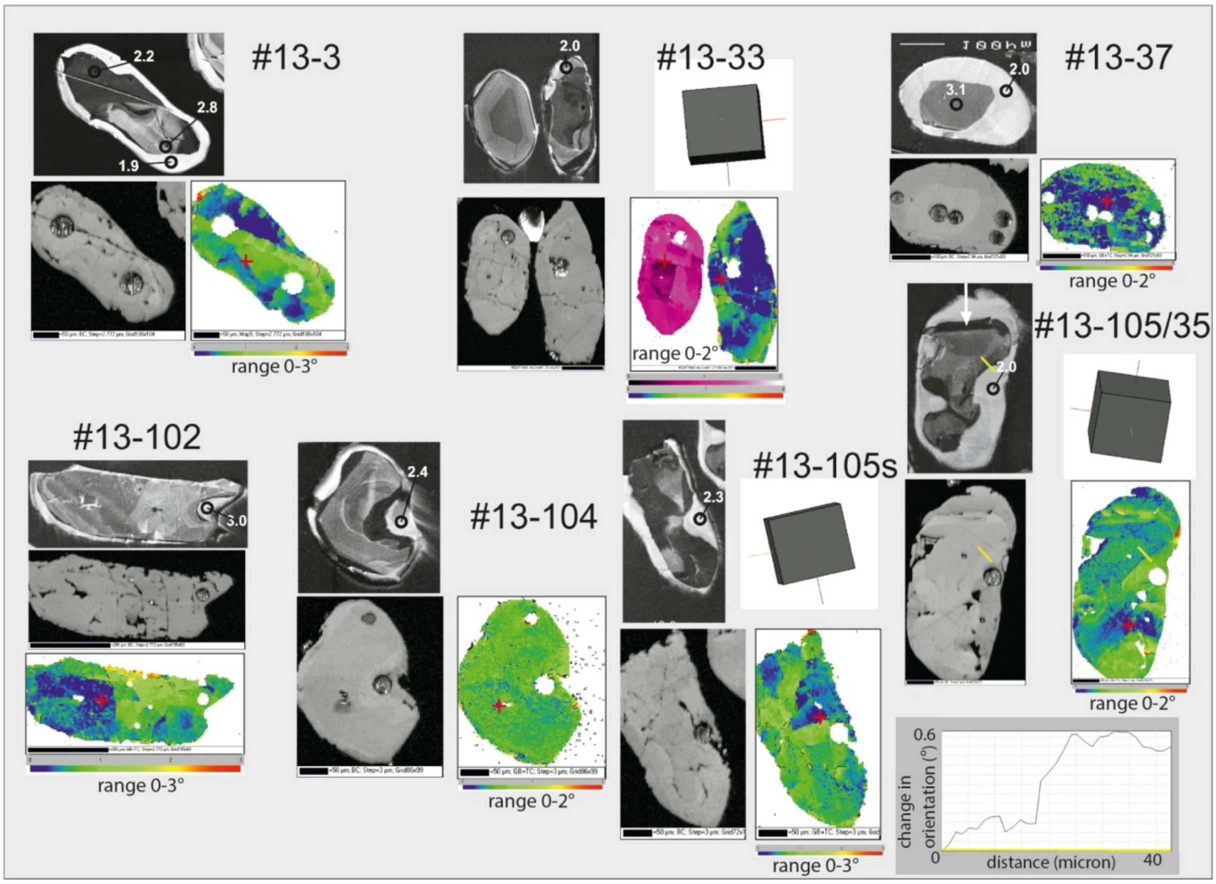

Fig. 12. Internal orientation relationships of selected zircon grains from the Gorbatovskaya 51 enderbite. For each grain the CL signal is shown on the top right, while the forescatter image is shown on lower right (or below – for grain #13-102). Colour maps are showing the change in crystallographic orientation from a reference point (marked with a red cross) shown from dark blue to red, or black to white (#13-22); the orientation range shown is 2° except for zircon #13-3 and #13-102 for which it is 3°. In these maps, subgrain boundaries with >1 orientation change between adjacent analysis points

are shown as magenta coloured lines. In some cases, the main crystal orientation is shown schematically in 3D (top right). For grain #13-105/35 orientation changes along a profile line crossing from the Cl-light rim to the dark border to the outer grain core (shown with white arrow). For further information on the technical details see explanations in the text and Appendix 1.

Grain # 13-37: There are two distinct CL zones identified for this grain: the dark core and the broad white rim. EBSD reveals that the boundary between the two is crystallographically controlled where the straight boundary is directly related to low index planes of the zircon core. Orientation changes are very minor and non-systematic, however, it is clear that the rim shows more crystallographic variation than the core.

Grain 13-102: This grain has a complicated structure with a high number of blocks of similar orientation suggesting brittle fragmentation and at least some immediate 'gluing" of the fragments to form a largely intact grain. However, some block boundaries are clearly associated with cracks that are currently observed in the forescatter image. This brittle deformation affected the whole grain except the CL-bright rim. This latter CL rim shows similar features to the #13-3 grain suggesting replacement and growth.

Grain #13-104: This grain is unusual compared to the other grains as it has no clear crystallographic orientation changes within the grain as shown by the homogeneous green colour of the EBSD map (left hand lower corner of image #13-104). There are no crystallographic characteristics that distinguish the rest of the grain from the core, which is distinct in the CL signal. However, in the forescatter image (right hand lower corner of image #13-104) the CL-black rim is clearly visible in the forescatter image as it is lighter grey than the rest of the grain. In the EBSD map only a minor difference in orientation is seen as reflected by slightly more blue and red orientations. The boundary between the CL-black rim and the CL-grey grain core is distinctly straight, similar to boundaries observed in other grains e.g. #13-105 and #13-33. At the same time, this boundary is at an angle to the CL-oscillations seen in the CL-grey core. The straight nature of the boundary suggests that this boundary is controlled by the crystal facet orientation. The fact that (a) dissolution of crystalline materials is crystallographically controlled (e.g. Godinho et al. 2012), and (b) the boundary and CL-occilations are not parallel, suggest that the CL-grey core was first resorbed to form crystal facets, and the black rim grew subsequently.

Grain #13-105s: The core and CL-grey outer part show blocks of similar orientation, with up to 1° rotation between grains suggesting brittle deformation and "gluing" similar to grain #13-102, however, in this case the CL-bright rim is unaffected by this brittle deformation. Noticeable is that the block formation seems to at least in part be controlled by crystallography, breaking preferable along crystal facets as the 2D traces of the block boundaries are consistent with crystal facet orientations (compare to orientation of 3D grain orientation, #13-105s image, upper right corner). The Cl-white rim, also distinct in the forescatter image, shows changes in crystallographic orientation with subgrain boundaries perpendicular to the CL-white and CL-back rim interface. The latter suggestions formation by replacement reaction.

Grain #13-105/35: In the forescatter image, this grain shows clearly topographic variations that are interpreted to be caused by subtle chemical variation between the grain parts. The original, magmatic core is the most resistant to mechanochemical polishing, standing relatively proud after polishing, as clearly visible on the forescatter image, while the CL-black rim is slightly lower in its resistance and the CL-bright rim is the most easily polished. Similar to #13-105s the CL-black rim seems to be associated with well-defined dissolution and then precipitation where the crystal facets are playing a major role. This is most evident at the top part of the grain (pointed to by white arrow in Fig. 12). Along with the growth of the black rim, some slight orientation change is seen which changes dominantly at the interface and parallel to the interface (see also profile that crosses from CL-white rim, to CL-black rim to core). The core exhibits a slight orientation variation with gentle lattice distortion probably due to crystal plastic deformation. The CL-bright rim is distinct as it exhibits a noticeable change in orientation to most of the crystal. However it should be noted that in places the orientation changes of the inner core are mirrored in the rim orientations i.e. the orientation changes of the core continue into the rim. Experiments by Spruzeniece et al. (2017), in which a grain that was pre-reaction plastically deformed was replaced by a fluid mediated replacement reaction, show the same "mirroring" of the original grain orientation changes into the replaced rim. This suggests that the plastic deformation of the core had taken place before the formation of the CL-bright rim.

4.2.3 U-Pb SIMS dating of zircon from the Gorbatovskaya 51 enderbite

U-Pb analyses using SHRIMP II (Appendix 1 methods) were conducted on both simple and complex zircon, including three sets of three analyses each on core – rim1 – rim2 (analyses 2, 3 and 14) and four core-rim couple of analyses (1, 9, 12 and 15). Analyses 1r, 2r2, 3r2, 9r, 13r, 14r2 and 15r were run on low CL overgrowths, while analyses 2r, 3r, 12r and 14r were conducted on brightly luminescent rims.

The common lead contents (*f*206, Table 4) are low, ranging from none to 0.89 %, while uranium and thorium concentrations range 14-434 ppm and 14-707 ppm respectively (Table 4, Fig. 13). Th/U ratios range from 0.12 to 1.75, and are not systematically different for the CL-black rims and some altered cores. The low uranium and thorium grains have yielded less precise results, though lesser degree of mitamictisation may mean less disturbance of U-Pb system.

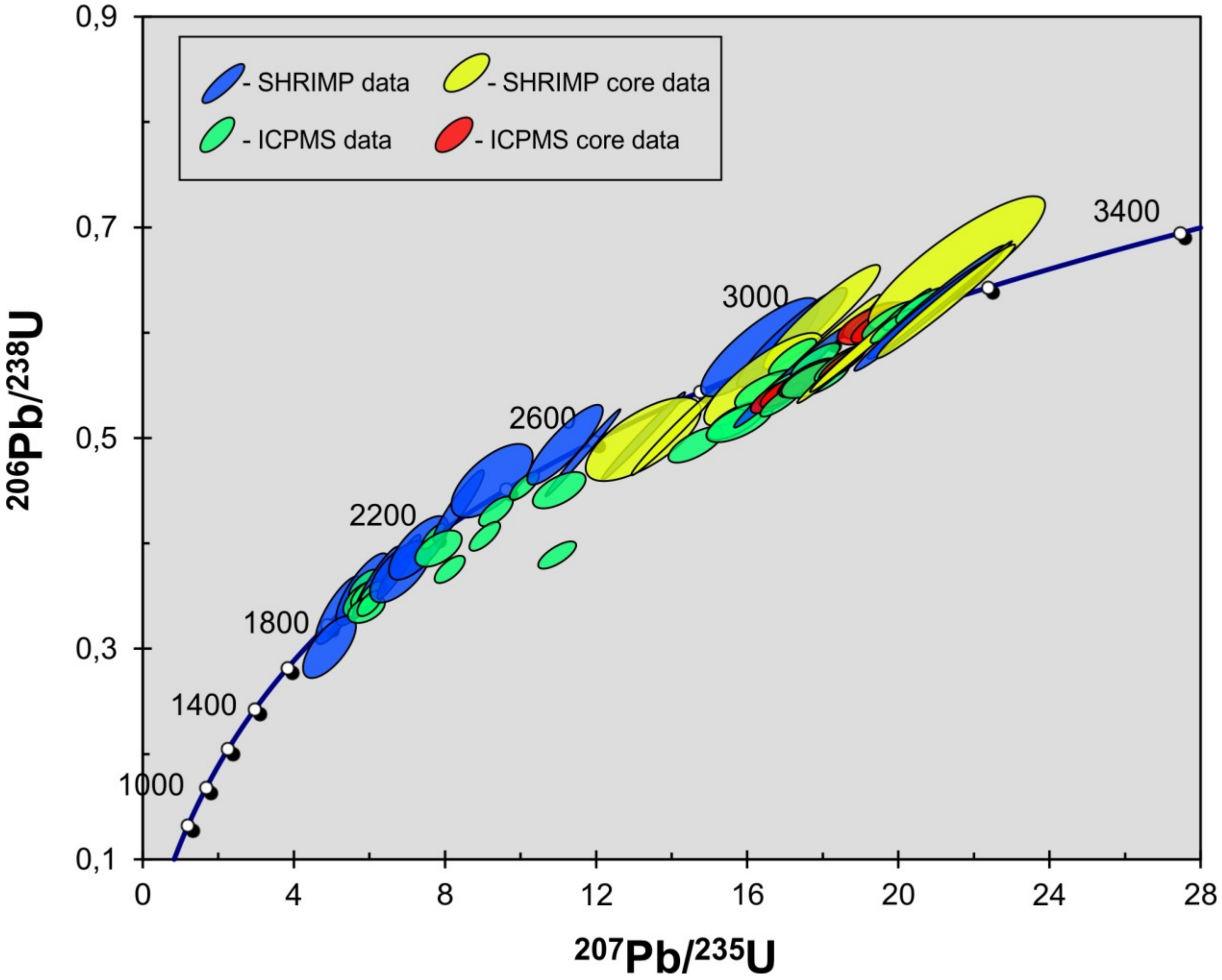

Fig. 13. U-Pb SHRIMP and LA ICPMS analyses of zircon from the Gorbatovskaya 51 enderbite of the Kolyvan suite.

The data range from slightly inversely to slightly normally discordant and define a wide spread of $^{207}Pb/^{206}Pb$ ages, ranging from 1814 ± 51 to 3151 ± 10 Ma (1σ errors, Fig. 13). The data on single-domain zircon and zircon core domains provide ages between 2086 ± 23 and 3151 ± 10 Ma. The CL-black (U-richer) inner rim analyses similarly define a wide range of ages between 2134 ± 55 and 3000 ± 10 Ma, while the outer, light CL (lower U) rims define imprecise ages of 1814 ± 51 to 1996 ± 28 Ma, with a weighted average of 1945 ± 130 Ma. The rims and cores may be interpreted to record a polyphase crystallisation history of the zircon, including possible thermal events at ca. 3.14, 3.1-3.0, 2.9-2.7, 2.6, 2.3-2.2 and finally 2.0-1.8 Ga. Alternatively, this spread of ages may reflect a continuous dissolution-precipitation process associated with replacement reactions that have led to incremental resetting of zircon U-Pb systematics. The youngest age of ca. 2.0-1.8 Ga is most probable the age of metamorphism, while the magmatic cores with oscillatory zoning yielded their maximum concordant age of 3151 ± 10 Ma. Clearly this rock has a complex radiogenic history that is difficult to resolve.

4.2.4 U-Pb LA-ICPM dating of zircon from the Gorbatovskaya 51 enderbite

A total of 38 U-Pb isotope analyses were done using the laser-ablation ICPMS technique (Table 4) that targeted zircon cores and rims which are at least 30 µm or wider. The location of the analytical points targeting different zircon domains is shown in Appendix 3. A large proportion of the analyses show a high degree of discordance (up to 30 %, Repository Table 5 and the Concordia diagram in Figure 13), which is mainly due to significant Pb-loss.

There are two major age populations that could be seen on the Concordia diagram in Figure 13: the older clustering between 3.0-3.1 Ga and a younger concordant or near-concordant population at around 1.95 Ga. When only the data collected on the core domains (n=12, excluding the most discordant grain #SVT13-30 Core) are used, the $^{207}Pb/^{206}Pb$ ages are between 3003 ± 44 to 3099 ± 42 Ma (2 sigma error) with the regression yielding an upper intercept age of 3092 ± 34 Ma (MSWD=2.5). If the rim data with ages over 2980 Ma are also used for the age estimate of the older population (n=30), the upper intercept age is slightly older at 3100 ± 22 Ma.

The youngest population of concordant or near-concordant (less than 10% discordant) data includes analyses on the outer rims with CL-bright response and a very low U content (mainly below 100ppm), which defines a relatively narrow range of imprecise ages from 1923 ± 116 to 2039 ± 84 Ma, with a weighted average of 1990 ± 37 Ma (MSWD=0.79; n=7). The eight most concordant analyses of the youngest CL-bright rims (Fig. 14 C) provide the Concordia age of 1950 ± 25 Ma.

There is also a scatter of CL-bright rim analyses with ages ranging between 2180 and 2623 Ma, but these are mainly discordant with only two near-concordant analyses at 2180 ± 58 Ma and 2461 ± 54 Ma.

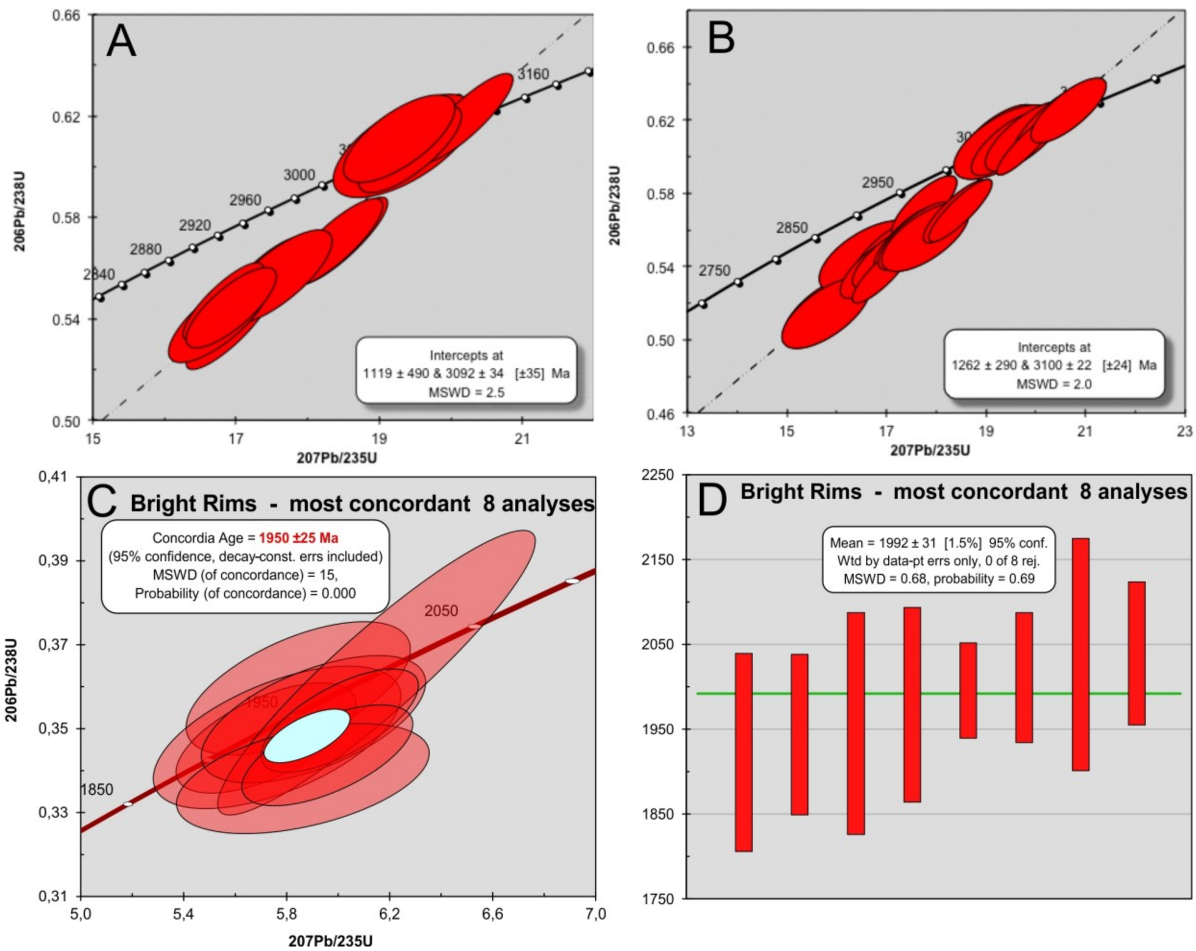

Fig. 14. U-Pb LA-ICPM data of zircon: older population, core analyses only (A), core and rim analyses over 2980 Ma (B); C and D - data of youngest 8 zircon rims.

4.2.5 Trace-element composition of zircon cores and rims

Th/U ratios and U concentrations. In the Gorbatovskaya 51 enderbite, Th/U ratios in the zircon magmatic cores range between 0.6 and 1.7, mainly 0.8-1.2 with Th contents varying between 60 and 707 ppm and U contents from 60 to 450 ppm (Tables 4, 5 and 6). These variations and positive correlation of Th and U contents may reflect changes in the zircon host melt following fractional crystallisation (e.g. Belousova et al., 2002). Departures from this trend match U-rich recrystallised cores. The CL-black and bright rims differ from the magmatic cores substantially in regards of their Th and U contents (see Fig. 15 and 14 A): the CL-black rims are relatively enriched in U (195-270 ppm), while the majority of the CL-bright rims are depleted down to 14-19 ppm. The Th/U ratios in the CL-bright rims are mostly within the 1.2-0.6 range, which characterise those with higher U contents. Some zircon grains, in which cores, CL-black and bright rims were analysed on the same grain (for example ##svt 13-1, 2, 3 in Table 4 and #SVT37, Table 5, Appendix 3) demonstrate that from cores to CL-black rims Th contents decrease but U - increase systematically. However, in the CL-bright overgrowth, both Th and U contents decrease. Many CL-bright rims plot closely to the main clusters of magmatic cores that can potentially be a result of sampling mixing due to the thin rim thicknesses (Fig. 14 A and Appendix 3). The absence of monazite and allanite in the studied enderbite may explain high Th/U ratio of the metamorphic zircon (e.g. Harley et al., 2007; Kirkland et al., 2015; Yakymchuk et al., 2018).

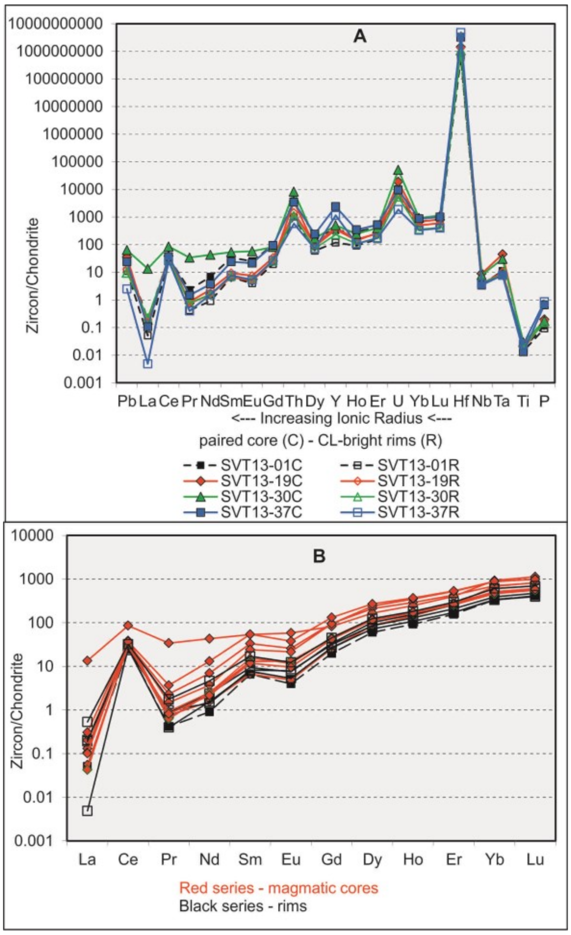

Fig.15. TE (A) and REE (B) patterns of zircon from the Gorbatovskaya 51 enderbite of the Kolyvan suite. Chondrite values are from Taylor and McLennan (1985).

Other trace and Rare Earth elements. Variations of trace elements in the magmatic cores are consistent with variations found in the outermost metamorphic rims (Fig. 15 A and B). Hf content in the magmatic cores varies notably from ca. 10,000 to 58,000 ppm (Table 6), probably mirroring the degree of fractional crystallisation. In contrast, the CL-bright rims appear to have slightly higher Hf and P, but lower Th, U and Y contents. The only analysed CL-black rim (#SVT13 01RIM in Table 6), in comparison, differs by lower concentrations of Hf and Y. However, the variation and distribution patterns of both cores and rims are similar with one exception in grain SVT-30C (Fig. 15 A).

Total REE contents in the zircon magmatic cores are significantly higher than in their rims: 1662 and 3316 ppm in the cores and 1147 to 2012 ppm in the rims (Table 6). The CL-black rim (#SVT 01RIM in Table 6) is the most REE depleted with noticeably lower Nd, Eu and some of the HREE contents (Fig. 15 B). Positive Ce and negative Eu anomalies are found in both the zircon cores and rims, that are a typical feature of all igneous zircon and also reported for grains of hydrothermal and metamorphic origin (Hoskin and Schaltegger, 2003).

Thus, the progressive recrystallisation of the primary magmatic zircon and formation of its rims correlates with depletion in REE, Th and U, which has been observed consistently in each analysed core-rim pair.

4.2.6 Zircon Hf-isotope results

Zircon Hf-isotope compositions were analysed on six zircon grains from the Gorbatovskaya enderbite (Appendix 3), where the rim and core domains were large enough to allow for multiple U-Pb and Hf-isotope analyses. The small size of the black CL rims restricted this work only to larger outer rims with bright CL. These data are collected on the zircon domains that yielded a near-concordant U-Pb age with the exception of a single analysis on the core of grain #37 with discordance of 15 %. A total of 12 analyses were done during two different analytical sessions in year 2010 and then in 2013. The Hf-isotope composition of studied grains shows a relatively narrow range of initial ^{176}Hf/^{176}Hf values from 0.280642 ± 16 to 0.280929 ± 12 (Table 7 and Figure 16). There is a clear trend of increasing initial ^{176}Hf/^{177}Hf ratios to more radiogenic values from cores to rims, with an average initial ^{176}Hf/^{177}Hf of 0.280751 ± 59 for the 6 core analyses and 0.280858 ± 91 for the 6 rim analyses.

When ƐHf is calculated using a measured $^{207}Pb/^{206}Pb$ age for the defined zircon domain, all of the analysed sampled produced negative $ƐHf_{(t)}$ values plotting well below the CHUR reference line (Fig.16). The $ƐHf_{(t)}$ of the magmatic cores ranges from -3.0 to -9.4, while metamorphic rims show a strongly evolved Hf-isotopic signature with $ƐHf_{(t)}$ values as low as -28 (ranging mainly from -14 to -28). The most conservative estimate of the age of the protolith for the Gorbatovskaya enderbite is provided by the T_{DM} model ages; they are ranging from 3.16 to 3.53 Ga with a mean of 3.32 Ga, while the crustal Hf model ages (T_{DM}^{C} in Table 7) give a range between 3.61 to 4.07 Ga for the age of the source. These values are consistent with the whole-rock Sm-Nd isotopic data for this enderbite and the Kolyvan granitoids (Table 2) giving $ƐNd_{(t)}$ ranging from -1.5 to -2.1 and T_{DM} ages of ca. 3.5 Ga. There is very little difference between the crustal Hf model ages of magmatic cores and metamorphic rims (3.66 Ga versus 3.75 Ga, respectively). On the $ƐHf_{(t)}$ versus U-Pb age diagram (Fig. 16B) both core and rim data plot closely to the same crustal evolution line with the age of around 3.75 Ga and $^{176}Lu/^{177}Hf$ ratio about 0.01. Their Hf-isotope composition and comparable Hf model ages imply Eo- to Palaeoarchaean crustal sources for the enderbitic magmas with the composition similar to that of the average Precambrian granitic crust ($^{176}Lu/^{177}Hf$ =0.0093; Vervoort and Patchett, 1996). There are very little, if any, juvenile additions during the metamorphic event at ca. 1945-1990 Ma recorded by the outer rims of the studied zircons.

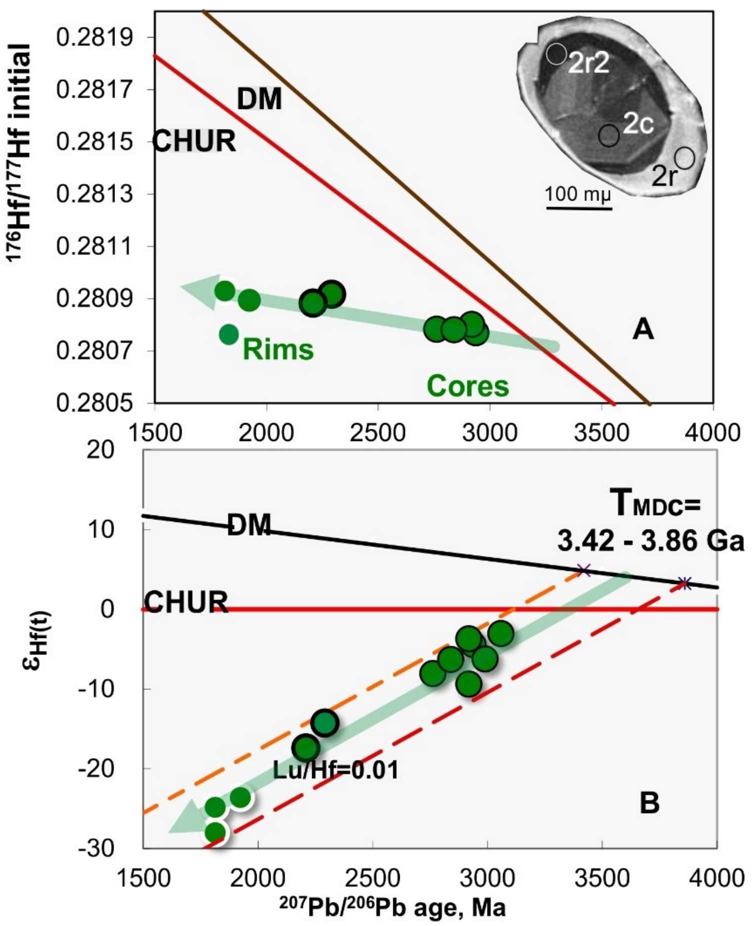

Fig. 16. Hf-isotope data vs $^{207}Pb/^{206}Pb$ age of zircon from the Gorbatovskaya 51 enderbite of the Kolyvan suite. A) $^{176}Hf/^{177}Hf$ initial, B) $\varepsilon Hf_{(t)}$. Rim analyses are shown as green circles with thicker darker rims; the points with the white rim are CL bright rim analyses (cf. Table 7). The domains visible under CL for grain #svt 13-2 shown in the upper right corner have been dated by SHRIMP targeting the core, CL black and bright rims with 2c, 2r2 and 2r analytical spots, given correspondingly in Table 4. The age of the core is reset due to recrystallisation. CHUR and DM evolution lines are according to Griffin et al., 2000. The evolution of ca 3.7 Ga crust is calculated assuming $^{176}Lu/^{177}Hf$ of 0.01, which is close to that of the average Precambrian granitic crust (e.g. $^{176}Lu/^{177}Hf$ of 0.0093; Vervoort and Patchett, 1996).

4.2.7 Zircon O-isotope results

Oxygen-isotope data obtained for the zircon analysed during this study show a relatively restricted range of $\delta^{18}O$ values, ranging from 4.4 to 6.4 ‰ (Fig. 17, Table 7), with an average of 5.8 ± 0.3 ‰ (1SD). The O-isotope values for the enderbitic zircon broadly overlap the range of typical mantle values of 5.3 ± 0.6 ‰ (2SE; Valley, 2003). There is no particular difference or correlation found in the O-isotope composition between the zircon core and rim analyses.

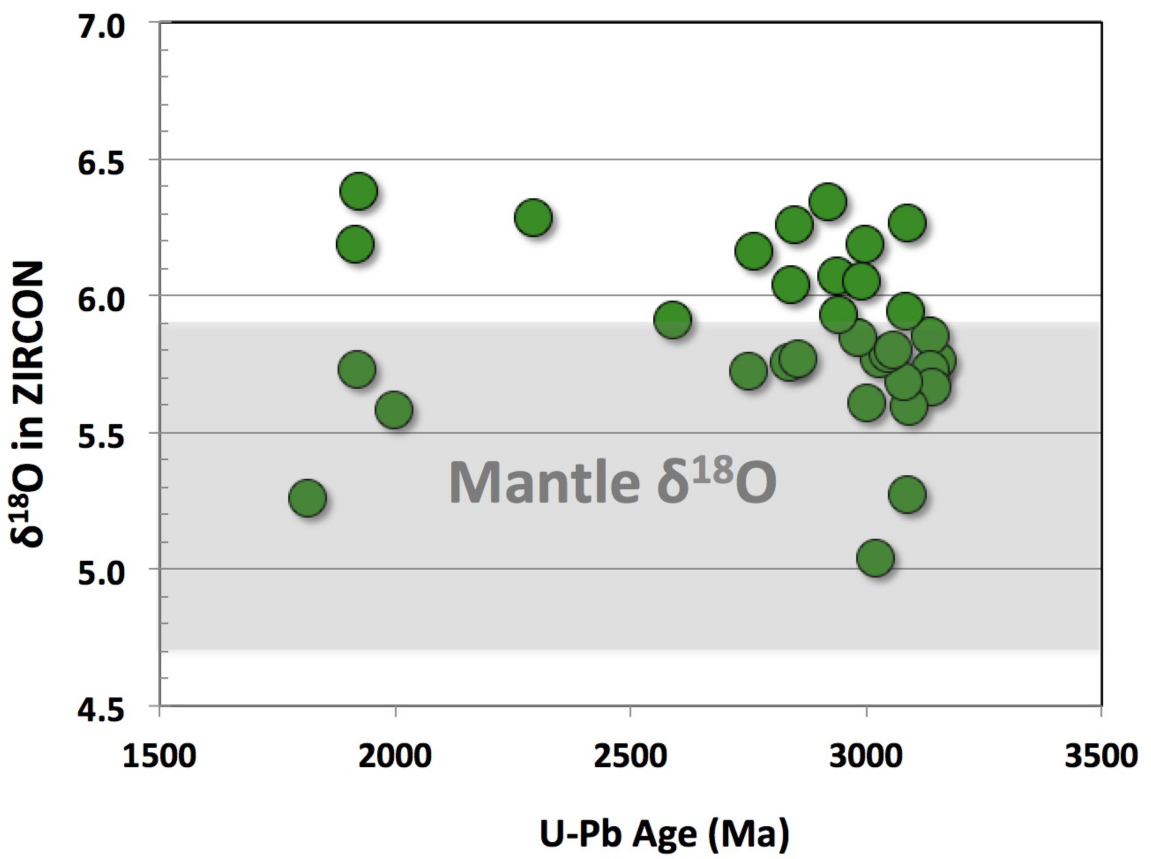

Fig. 17. $\delta^{18}O$ *versus U-Pb age for zircon from the Gorbatovskaya 51 enderbite of the Kolyvan suite.* $\delta^{18}O$ *values are quoted in per mil (‰) with respect to Vienna Standard Mean Ocean Water (VSMOW).*

5 Discussion

5.1 Palaeoproterozoic metamorphism, deformation and zircon growth

5.1.1 Petrographic data

As described above, almost all Kolyvan charnockitoids are variably sheared and were subjected to high-grade metamorphism. Their metamorphic assemblage is orthopyroxene ± diopside + amphibole + biotite + plagioclase + quartz, which is similar to that of the magmatic charnockitoids and granitoids. The absence of garnet makes it difficult to estimate the PT parameters of metamorphism. Also, hypersthene, which could be used for the evaluation of the metamorphic P-T conditions, has the same composition in the primary magmatic and in the sheared enderbites (Appendix 4).

Of particular interest are zones of severe amphibolitisation in the magmatic enderbites, which are 2-10 cm wide and discordant to the enderbite fabric (Figs. 2 and 9). According to the conventional classification (Leake et al., 1997), the amphibole (Appendix 4) belongs to the hastingsite group and occurs together with andesine (An 35-40), diopside, biotite, quartz, magnetite and ilmenite. The two latter are products of exsolved magmatic Ti-magnetite, which is characteristic for the initial magmatic enderbites. Amphibole-plagioclase geothermobarometers (Molina et al., 2015) and the Al-in hornblende barometer (Van Kranendonk et al., 2015) all indicate that the amphibolitisation and deformation of the charnockitoids took place at 700-750ºC and 4-5 kbar which probably characterise a retrograde stage.

Metamorphism and deformation of the Kolyvan igneous rocks occurred at 700-750°C and 4-5 kbar as a minimum. The difference in the PT conditions during magma crystallisation at 3.1 Ga and metamorphism at 1.95 Ga implies that after emplacement and crystallisation of the Kolyvan pluton the Mesoarchaean lower crust was uplifted by 10-12 km but remained within high amphibolite- to granulite facies retaining the HT/LP regime.

5.1.2 Deformation and metamorphic zircon growth

The magmatic, oscillatory zoned cores rarely preserve their euhedral crystal morphology, their edges are irregular, angular or variously curved. Internally, some original magmatic cores with oscillatory zoning show «ghost» and faded textures due to recrystallisation (Corfu et al., 2003). They display various CL responses: grey, black or bright (Figs. 11, 12 and Appendix 3).

Cores are enveloped by inner CL-black and outer CL-bright rims. The rims are sharply discordant to the core zoning, resorbing and replacing the latter. The CL-bright rims (up to 80 µm thick, defining the ovoid morphology of the zircon grains and in some grains these rims cut off the discontinuous CL-black rims and lobes). Within the CL-bright rims, greyish shadows appear to continue into pre-existing shapes of the black rims (see various grains in Fig. 11 and Appendix 3). These structural rim-rim relationships indicate that the CL-bright rims formed last in the zircon growth. However, the question remains as to whether these intimately related rims developed during different events or close in time when the CL-bright rims were growing due to solid-state diffusion or dissolution-precipitation reactions of the magmatic cores and the CL-black rims. With regard to solid-state recrystallisation, the CL-black rims enriched in U potentially represent a reaction front between the magmatic cores and the newly forming lower U metamorphic overgrowths as was suggested in previous studies (e.g. Hoskin and Black, 2000).

The EBSD study of the enderbitic zircon (section 4. and Fig. 12) resolves that a) the magmatic cores were affected by crystallographic disorientation due to fracturing and “re”gluing (Rimsa et al. 2007, Tretraikova et al. 2017) and possibly some minor crystal plastic deformation before the CL-bright rims grew; b) the CL-black rim seems to be associated with well-defined dissolution and then precipitation where the crystal facets are playing a major role. Experiments on minerals such a fluorite show that dissolution is highly anisotropic with dissolution being much slower at crystal facets than other boundaries. This then results in the preferential "preservation" of facets (e.g. Godinho et al., 2012). Accordingly, the old magmatic zircon (now forming cores) where subject to significant dissolution before a relatively homogeneous black rim formed. The exact timing of the two phases – dissolution versus new growth – is not clear, however, these two processes do not seem to have been coupled. There is, therefore a significant time difference involving two separate fluids/melts, one that was highly undersaturated in Zr, triggering dissolution, and one that was oversaturated and U rich, triggering growth.

The CL-bright rim is distinct as it exhibits a clear change in orientation to other domains of the crystals (Fig. 12). However, it should be noted that in some places its crystallographic orientation mimics the orientation of the inner core, similar to the cases observed in previous studies (Spruzeniece et al., 2017). Different to the black rim, there is a clear feature that is associated with coupled dissolution and precipitation replacement reactions i.e. subgrain boundaries that emanated from the reaction interface (i.e. CL-white-core/black rim interface) (Fig. 12).

In regards to changes in chemical compositions, the rims differ markedly from those of the magmatic cores by lower Th, U, Pb, Y and REE concentrations (Figs. 14 and 15), but by higher Hf and P, the latter two typically elevated in late-magmatic zircon outer domains (Belousova et al., 2002). The CL-black rims are particularly enriched in U, having Th/U ratios below 0.6 (Fig. 14), whereas the CL-bright outer rims plot either closely to the main Th/U clusters of magmatic cores or are in the field of data showing relative depletion in U.

In summary, after the magmatic crystallisation, the enderbitic zircon experienced severe modifications responsible for formation of the double CL-black and bright rims. Being metamorphic, they differ from the cores in chemistry and internal structure and appear to develop through two discrete events, the CL-black rims at first and the CL-bright ones after. Each of them shows its own orientation changes and probably formed by diverse mechanisms (Geisler et al., 2007). Fluid-mediated dissolution-precipitation with variable apparent inward-penetrating textural features may have prevailed when the CL-bright rims formed. For the CL-black rims, significant dissolution predating later growth is most consistent with the data collected. It is also noteworthy that the CL-black rims do not show any signs of typical metamict structures. In contrast, thin brittle fractures seemingly filled with the CL-bright materials are present indicating once more that the growth of the CL-bright rims took place during a separate event (Figs. 11 and 12; Appendix 3). The diverse mechanisms (i.e. brittle and crystal plastic deformation, dissolution and growth, fluid-assisted replacement reactions) resulted in intercrystalline defects e.g. dislocation arrays within the different zircon domains. Such defects have been shown to accelerated trace-element diffusion by pipe diffusion (e.g. Piazolo et al. 2016). Accordingly, age and chemistry of zircons may have been modified significantly.

5.2 U-Pb zircon data in the context of magmatic and metamorphic events in the history of the Kolyvan suite

The U-Pb isotope studies of zircon allow recognition of at least two stages of the Kolyvan suite formation.

The early stage ca 3.15 billion years ago was responsible for the formation of magmatic protoliths of the rocks of the complex. For the Gorbatovskaya 51 enderbite the oldest age of the magmatic cores is defined between 3151 ± 10 Ma (SHRIMP) and 3118 ± 48 Ma (LA-ICPMS). Thus, there is a good agreement between SHRIMP and LA-ICPMS U-Pb age results (Fig. 13) suggesting that the maximum crystallisation age of the magmatic cores in zircon from the Gorbatovskaya 51 enderbite is as old as 3150 Ma. The spread towards the younger ages is most likely due to Pb-loss. Related to the Kolyvan enderbites, granitoids from two localities yield consistent ages for magmatic zircon of 3131 ± 7 Ma and 3137 ± 15 Ma (section 4.1, Figs. 9 and 10) that are similar within analytical errors to the age of crystallisation of the enderbites. The fractures observed in these cores (Fig. 11) may explain some of the age ranges observed due to associated Pb-loss.

The late stage about 1.95 billion years ago was marked by large-scale metamorphism of the magmatic protoliths. This event is recorded by the CL-bright rims and dated between 1945 ± 130 Ma (SHRIMP) and 1990 ± 37 Ma (LA-ICPMS): The most concordant analyses provide the most reliable estimate for the time of the formation of the CL-bright rims at 1950 ± 25 Ma (Fig. 14 C). Microstructurally, this event shows a distinct texture typical for replacement reactions with subgrain boundaries/orientation changes perpendicular to the rim-core interface, where zircon in disequilibrium with the surrounding fluid was dissolved and zircon in equilibrium (i.e. new age) grew instead (Putnis, 2019, Spuziernce et al. 2017). Such dissolution-precipitation of zircon suggests that the U-Pb systematics is not completely reset causing the relatively wide spread of ages (Spruzeniece et al., 2017). It is also possibly that recrystallisation in dry conditions may also result in an incomplete U-Pb resetting (e.g. Wan et al., 2011).

The CL-black rims produce a wide range of dates between 2751 ± 17 Ma and 2134 ± 110 Ma (SHRIMP). This scatter is interpreted as a result of various degrees of Pb-loss and re-equilibration of the magmatic zircon U-Pb system. The fact that commonly the interface between the core and the black rim is very sharp and controlled by the crystal lattice i.e. parallel to a zircon facet orientation, suggests that significant dissolution took place (e.g. Godinho et al. 2012) before new zircon with a distinctly different chemistry grew. Just like for the white rims, a spread of ages would be expected. Moreover, secondary thermal events such as at 2291 ± 62 Ma and 2208 ± 21 Ma concordant or near-concordant analyses (SHRIMP) and 2461 ± 54 Ma and 2180 ± 58 Ma (LA-ICPMS) could not be completely disregarded considering known magmatic event in the studied area, including 2.2-2.1 Ga magmatism in the adjacent Volga-Don Orogen, East Voronezh massif (Terentiev et al., 2014; Terentiev et al., 2016). In summary, the CL-black rims could be formed either a) at 2461 ± 54 Ma and subjected later to U-Pb resetting in the magmatic cores, before or during the CL-bright rim developed at ca. 1.99-1.95 Ga or b) the obtained concordant analyses and their clustering respond to separate tectono-thermal episodes.

5.3 Origin and tectonic setting of the igneous protolith of rocks of the Kolyvan suite.

5.3.1 Some speculations on the origin of the Kolyvan charnockitoids and related granitoids

High variations of major elements and their departures from linear trends are notable for the Kolyvan charnockitoids and granitoids (Figs. 5 and 6). Whether this is due to different compositions of melt sources, assimilation of crustal rocks, mechanism of crystallisation or superimposed metamorphism is difficult to distinguish. Several observations should be considered:

a) Geologically, two suites, namely Kol 1 and Kol 2, are recognised, each showing distinct major and trace elements variations (Figs. 4, 6 and 7). Particularly, the Kol 2 rocks show much higher abundances of Rb and ΣREE. The Kol 2 charnockitoids have higher $LREE_N/HREE_N$ (59-127) than those of Kol 1 (16-42) as well as other ratios (Table 1). Even though the Kol 1 and Kol 2 rocks represent separate suites, this does not preclude that Kol 2 represents a residual melt after the major crystallisation of the Kol 1 suite;
b) The compositional variations of the Kolyvan charnockitoids and granitoids were probably determined by magma differentiation both at the level of its emplacement (garnet-free crystallisation), where the cumulative gabbro-anorthosites were formed, and at deeper levels in garnet field stabilisation producing rock types with low contents of HREE.
c) Enclaves of mafic compositions and inclusions of euhedral plagioclase (Fig. 2) in some of the Kol 1 rocks indicate mingling of mafic and granitoid melts; the gabbronorite (sample 81-1, Table 1) has different major and trace geochemistry and probably represented a separate mafic melt;
d) P-T conditions for crystallisation of the Kolyvan melts could be roughly estimated to less than 7-9 kbar pressure, accounting for the garnet absence along with contents of pressure dependent trace elements (Sr and Y) (Fig. 8). The granitoid melts crystallised at shallower levels with decreasing temperature. Assuming that rocks do not represent cumulates and/or experienced loss of mobile elements, melt liquidus temperatures calculated by the NORM4 Excel facility (www.earthchem.org) vary from 1072ºC to 861 ºC (16 analyses) for the Kol 1 enderbites, from 1097 ºC to 901ºC (6 analyses) for the related granitoids and from 875ºC to 810ºC (13 analyses) for the Kol 2 charnockites. Similarly, Brey and Köhler's experimental TCa-In-opx geothermometer (Brey and Kohler, 1990) gives 880-1030ºC,

mostly 960ºC for the enderbite crystallisation. Thus, the reasonable temperatures of the magma crystallisation of the charnockitoids and granitoids range between 1000 and 900°C. Such melting and crystallisation temperatures for the Kolyvan charnockitoids could be provided by a geotherm of about 30°/km (Moyen, 2011). Employing the zircon saturation approach (Watson et al., 2006), the crystallisation temperature for the Kol 1 enderbites is 750-830ºC and ca. 770ºC for the Kol 2 charnockites. The lower temperatures 590-720ºC overprint petrographic features in deformed enderbites, which may have affected zircon ages by fluid mediated replacement reactions where zircon is dissolved and immediately reprecipitated with a mixed age signature. The Ti-in-zircon crystallisation temperature (Watson and Harrison, 2005) of the Gorbatovskaya 51 enderbite scatters between 731 and 803ºC independently of spot location either in cores or in rims (Table 2) which could it be due a local Ti remobilization to presence of micro-inclusions or in cracks or in metamict U-rich zones or domains.

e) Compared with worldwide charnockites *s.l.* (Frost and Frost, 2008), the Kolyvan rocks exhibit compositions of both ferroan and magnesian suites and a peraluminous trend of ASI decreasing with increasing SiO_2 that is not typical for other charnockitic plutons with some exceptions. The peraluminous character of the Kol 1 suite and its medium- to high K_2O fields (Fig. 5) might signal that cumulative processes during plagioclase crystallisation were important, but this remains to be solved by detailed petrological work;

f) Low-silica (SiO_2 < 60 wt. %) enderbites of the Kolyvan 1 suite are too mafic to be generated during crustal melting. They were rather formed due to melting of mafic or ultramafic sources or due to differentiation of a more mafic "initial" melt. Gabbronorite found as a mingling inclusion among rocks of the Kol-1 suite is not suitable for the role of such an "initial" melt, since it has very low concentrations of Zr, Nb, LREE and a weakly fractionated HREE pattern. A more likely example of the "initial" Kolyvan suite melt is the

Kol-93-15 sample. It has the highest MgO, FeO and TiO_2 concentrations, relatively low Al_2O_3 contents, and is probably the least enriched in cumulus plagioclase. This sample records low magnesium (Mg # = 45) and it is probably a product of crystallisation differentiation of a more primitive mantle equilibrium magma. We do not have samples of the primitive magma, but geochemical features of sample Kol-93-15 allow us to estimate the original conditions and geochemistry of its mantle source. Strong fractionation of heavy REEs indicates the melt generated in equilibrium with garnet-bearing restite, which suggests a pressure of about 25 kbar (Grove et al., 2013) or at a depth of about 90 km. High concentration and strong fractionation of light REE, and sharp negative Nb-anomalies indicate that the mantle source of the melt has undergone metasomatic alterations. These alterations, according to isotopic data, took place in the Palaeoarchaean between 3.5 Ga (WR T_{DM}Nd) and 3.75 Ga (T_{DM}Hf-in zircon, long before the Mesoarchaean Kolyvan magmatism 3.15 Ga (U-Pb-in zircon). The presence of a 3.3 Ga zircon xenocryst in the Kolyvan granitoids suggest that Palaeoarchaean crust was involved to the Kolyval suite genesis. $\delta^{18}O$ values in the enderbite zircon, ranging from 4.4 to 6.4 ‰ with an average of 5.8 ± 0.3 ‰ (1σ), imply that no supracrustal rocks were involved in the source of the Kolyvan melts.

To summarise, the Kolyvan charnockitoids and granitoids appear to belong to a comagmatic I-type granitoid series, crystallised at the level of the middle- to lower crust (ca. 25 km depth) 3.1-3.2 Ga ago. The overall composition of the rocks and their isotopic characteristics (O and Hf-in-zircon, whole rock εNd) suggest that the Kolyvan melts originated from pre-existing Eo- to Palaeoarchaean lithoshere. At the emplacement level, fractional crystallisation was the prevailing mechanism for the rock formation.

5.2.2 Geodynamic setting of Kolyvan magmatism

The data on the possible origin of the Kolyvan magmatism suggest that the Kolyvan charnockitoids formed in a geodynamically active environment with high geothermal gradient of ca. 30°C/km, probably under the influence of asthenospheric basaltic magma. The melts originated from a crustal or enriched mantle source, which was formed 3.5-3.8 Ga ago, i.e. long before the episode of melting and formation of the Kolyvan magmas ca 3.1 Ga ago. The emplacement and final crystallisation of the Kolyvan charnockitoids and granitoids took place at low-to-medium pressure, corresponding to the level of ca. 25 km, indicating that continental crust of near modern day thickness already existed in Volgo-Uralia at 3.1-3.2 Ga. All these petrological inferences can serve as constraints on the possible geodynamic setting of Kolyvan magmatism.

A consensus is that the global geodynamics profoundly changed at 3.0-3.2 Ga, when the first evidence of modern-style plate tectonics is recorded (Dhuime et al., 2012; Moyen, Laurent, 2018; Pease et al., 2008; Cawood et al., 2018). If so, Kolyvan magmatism could mark a convergent setting at the edge of an ancient continental plate, such as an active margin by analogy with charnockitic magmatism in the Dharwar and other Archaean cratons in India (Rajesh, 2012), or a back-arc basins along an active continental margin (Hyndman et al., 2005) that may explain the high-T, dry and ferroan- to magnesian magmatism as seen in the Kolyvan suite.

On the other hand pre-plate tectonics, with melting of a delaminated lithosphere and of a upwelling astenospshere together with mantle-plume activity at 3.1-3.2 Ga (Cawood et al., 2018) could have caused mantle underplating, extension of the Palaeoarchaean crust, its melting and high-T magmatism. Asthenosphere upwelling and lithosphere extension due to an arrival of a deep mantle plume appears preferable also in the context of thermomechanical modelling of the Earth evolution by ca. 3.0 Ga (Gerya et al., 2015; Sizova et al., 2015).

Discriminant geochemical diagrams provide a contradictory estimate of tectonic setting (fig. 18). Some geochemical features such as a low concentrations of Rb, Y, Nb and heavy REEs, are typical for island arc environments. On the other hand, the high concentrations of light REE and Zr in most rocks brings them closer to the A-type granites, which suggests their connection with intraplate environment and the leading role of mantle plumes.

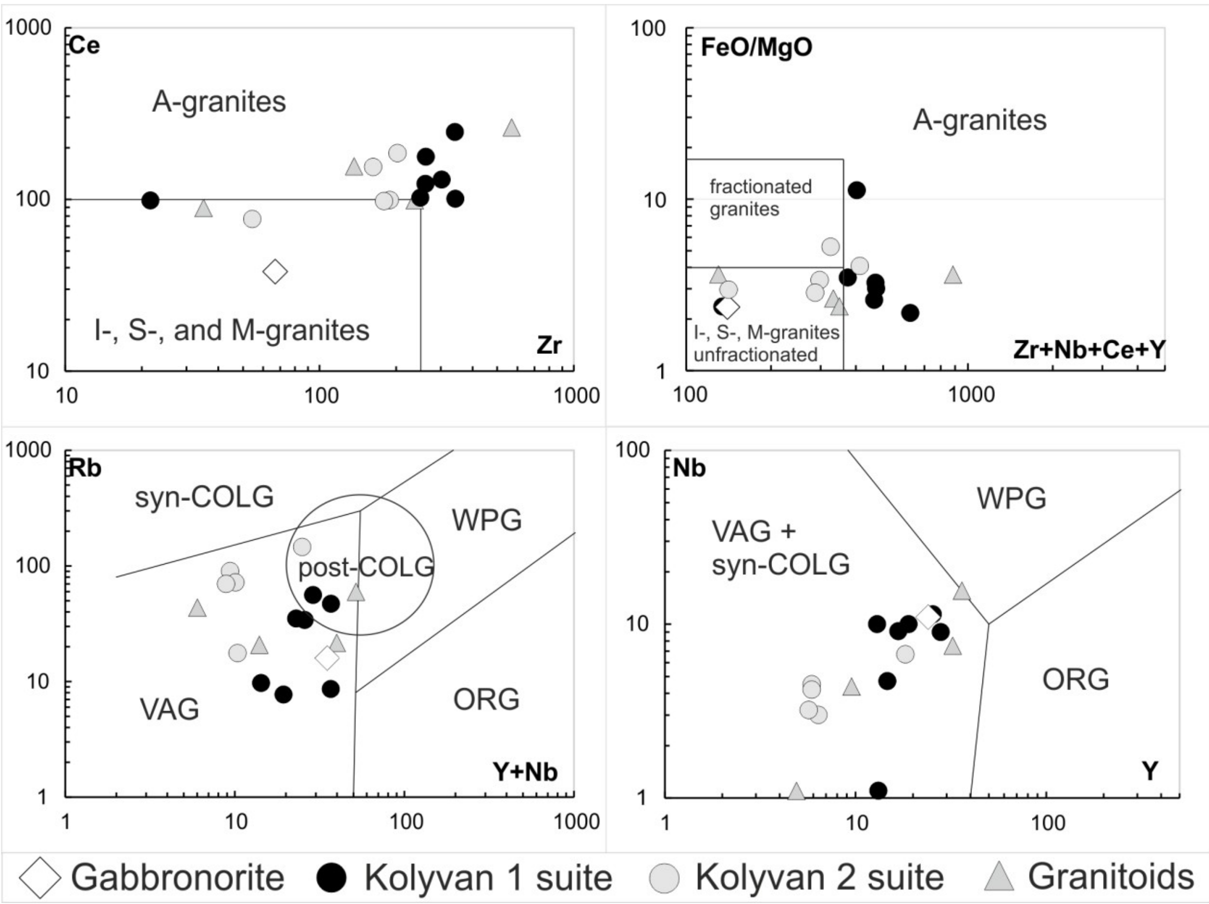

Fig. 18. Discriminant diagram (Pearce et al., 1984; Pearce, 1996; Whalen et al., 1987) for Kolyvan rocks

Petrology of the Kolyvan low-SiO_2 primitive magmas, considered above, provides additional arguments for discussing the geodynamic setting of the Kolyvan magmatism. The formation of the Kolyvan primitive magmas due to melting of the older metasomatised mantle is difficult to reconcile with a convergent tectonic setting, because in this metasomatism and melting of the lithospheric mantle events are closely spaced in time, ensuring the formation of melts with juvenile isotopic characteristics. The model of melting of ancient metasomatised continental lithosphere under the influence of an asthenospheric plume looks more consistent. Gabbronorites, which are present in the Kolyvan Group, but contrastingly differ from it in geochemical features, may represent remnants of this plume magmatism.

Thus, the obtained data can be most fully consistent in a model in which mantle-plume activity at 3.1-3.2 Ga caused mantle underplating, extension of the Palaeoarchaean lithosphere, its melting and high-T magmatism.

Conclusions

1. In the southwestern part of the Volga-Uralia segment, in the Middle Volga megablock, enderbites and associated granitoids of the Kolyvan complex are widespread and carry information on the Meso- and Palaeoarchaean history of this segment of the continental crust.

2. The age of the protoliths based on U-Pb isotope dating of magmatic zircon cores is ca 3150 Ma.

3. The Nd model ages of granitoids (TNd_{DM} = 3.46 Ga), zircon Hf model ages (THf_{DM} = 3.32 - 3.53 Ga), as well as zircon U-Pb age of 3.3 Ga, indicate that the Mesoarchaean granitoids of the Kolyvan complex were formed during melting of the Eo- to Palaeoarchaean metasomatised lithospheric mantle and continental crust sources.

4. The Kolyvan low-SiO_2 primitive magmas could be generated via a melting of the ancient metasomatised continental lithosphere under the influence of an asthenospheric plume. The plume-derived magmas may be represented by gabbronorites, which are recognised in the Kolyvan suite, but contrastingly differ from it in geochemical features.

5. Structural and metamorphic modification of the granitoids occurred 1.95 Ga ago under conditions of T = 700 - 750 ^{0}C and P = 4 - 5 kbar. This process led to the formation of high-temperature mylonites and also left characteristic imprints in metamorphic zircon, such as distinct Cl-rims characterised by a clear chemical signature along with microstructural features associated with fluid mediated replacement reactions.

Acknowledgements

This work was supported by the Australian Research Grant FT110100685 to E.Belousova and FT110100070 to S. Piazolo, IGEM RAS grant AAAA-A18-118021990105-9 to A.V. Samsonov. These sources of support are gratefully acknowledged.

Samples for this research were provided from the museum collection of the Department of Lithology, Gubkin State University of Oil and Gas, Moscow, Russia. Analytical data were obtained using instrumentation funded by DEST Systemic Infrastructure Grants, ARC LIEF, NCRIS and Macquarie University, Karpinsky Russian Geological Research Institute. The authors acknowledge the facilities, and the scientific and technical assistance of the AMMRF at CMCA-UWA, a facility funded by the University of Western Australia, State and Commonwealth Governments. This is contribution XX from the ARC Centre of Excellence for Core to Crust Fluid Systems (www.CCFS.mq.edu) and XXX from the GEMOC National Key Centre (www.GEMOC.mq.edu.au).

We are indebted to A. Shchipansky and two anonymous experts for thorough reviews that helped improve the original version of the manuscript.

References

Artemieva, I.M., Mooney, W.D., 2002. On the relations between cratonic lithosphere thickness, plate motions, and basal drag. Tectonophysics 358, 211-231.

Bédard, J.H., 2018. Stagnant lids and mantle overturns: Implications for Archaean tectonics, magmagenesis, crustal growth, mantle evolution, and the start of plate tectonics. Geoscience Frontiers 9, 19-49.

Belousova, E. A., Walters, S., Griffin, W. L., O'Reilly, S. Y. & Fisher, N.I., 2002. Igneous zircon: trace element composition as an indicator of source rock type. Contributions to Mineralogy and Petrology, 143, 602-622.

Bibikova, E.V., Bogdanova, S.V., Kirnozova, T.I., Popova, L.P., 1984. The uranium-lead age of charnockitoids in the Volga-Urals province. Doklady (Transactions) USSR Acad. Sci. 276 916-919.

Bibikova, E.V., Bogdanova, S.V., Postnikov, A.P., Fedotova, A.A., Claesson, S., Kirnozova, T.I., Fuzgan, M.M., Popova, L.P., 2015. The oldest crust of the Volgo-Uralian segment of the East European Craton: an isotope- geochronological study of detrital zircon from metasedimentary rocks of the Bolshoy Cheremshan Group and their Sm-Nd model ages. Stratigraphy and Geological Correlation 23, 1-23.

Bibikova, E.V., Bogdanova, S.V., Postnikov, A.V., Popova, L.P., Kirnozova, T.I., Fugzan, M.M., Glushchenko, V.V., 2009. Sarmatia-Volgo-Uralia junction zone: Isotopic-geochronologic characteristic of supracrustal rocks and granitoids. Stratigraphy and Geological Correlation 17, 561-573.

Bibikova, E.V., Kirnozova, T.I., Popova, L.P., Postnikov, A.V., Makarov, V.A., Kremenetsky, A.A., 1994. U-Pb ages and correlation magmatic rocks of granulite- and amphibolite-facies complexes in the Volgo-Uralian Province of the East European Craton. Stratigraphy. Geological Correlation 2(3), 3-7.

Bleeker, W., 2003. The late Archean record: a puzzle in ca. 35 pieces. Lithos 71, 99-134.

Bogdanova, S., Gorbatschev, R., Grad, M., Guterch, A., Janik, T., Kozlovskaya, E., Motuza, G., Skridlaite, G., Starostenko, V., Taran, L., 2006. EUROBRIDGE: New insight into the geodynamic evolution of the East European Craton in: Gee, D.G., Stephenson, R.A. (Eds.), European Lithosphere Dynamics, Geological Society, London, Memoirs, 32. Geological Society London, pp. 599-628.

Bogdanova, S.V., 1986. The Earth's Crust of the Russian Platform in the Early Precambrian (as exemplified by the Volgo-Uralian segment). Nauka, Moscow. 224 p.

Bogdanova, S.V., 1993 Segments of the East European Craton in: Gee, D.G., Beckholmen, M. (Ed.), EUROPROBE in Jablonna 1991. European Science Foundation - Polish Academy of Sciences pp. 33-38.

Bogdanova, S.V., Belousova, E.A., De Waele, B., Postnikov, A.V., 2013. Zircon from Mesoarchean enderbites of Volgo-Uralia: U-Pb age, REE, Hf and O-isotope compositions, Goldschmidt 2013, Mineralogical Magazine ed, Florence, p. 727.

Bogdanova, S.V., Bingen, B., Gorbatschev, R., Kheraskova, T.N., Kozlov, V.I., Puchkov, V.N., Volozh, Y.A., 2008. The East European Craton (Baltica) before and during the assembly of Rodinia Precambrian Research 160, 23-45.

Bogdanova, S.V., De Waele, B., Bibikova E.V., Belousova, E.A., Postnikov, A.V., Fedotova, A.A., Popova, L.P., 2010. Volgo-Uralia: the first U-Pb, Lu-Hf and Sm-Nd isotopic evidence of preserved Paleoarchean crust. American Journal of Science 310, 1345-1383.

Bogdanova, S.V., Gorbatschev, R., Garetsky, R.G., 2016. EUROPE|East European Craton, in: Scott, E. (Ed.), Reference Module in Earth Systems and Environmental Sciences. Elsevier.

Bogdanova, S.V., Lapinskaya, T.A., Postnikov, A.V., 1978. Metamorphic complexes of the basement of the eastern Russian platform, in: Dagelaysky, V.B., Bondarenko, L.P. (Eds.), Metamorpic complexes of the basement of the Russian platform. Nauka, Leningrad, pp. 156-198.

Bogdanova, S.V., Postnikov, A.V., Bibikova, E.V., 2012. The Volga-Don orocline stitching Volgo-Sarmatia. Geophysical Research Abstracts 14, EGU2012-11762.

Brey, G.P., Kohler, T., 1990. Geothermobarometry in Four-phase Lherzolites II. New Thermobarometers, and Practical Assessment of Existing Thermobarometers. Journal of Petrology 31, 1353-1378.

Brown, M., 2008. Characteristic thermal regimes of plate tectonics and their metamorphic imprint throughout Earth history: When did Earth first adopt a plate tectonics mode of behavior?, in: Condie, K.C., Pease, V. (Eds.), When did plate tectonics begin on planet Earth? Geological Society of America, Boulder, USA, pp. 97-128.

Cawood P.A., Hawkesworth C.J., Pisarevsky S.A., Dhuime B., Capitanio F.A., Nebel O. 2018. Geological archive of the onset of plate tectonics. *Phil. Trans. R. Soc. A* **376**: 20170405.

Collins, W.J., 2002a. Hot orogens, tectonic switching, and creation of continental crust. Geology 30, 535-538.

Collins, W.J., 2002b. Nature of extensional accretionary orogens. Tectonics 21, 6-1-6-12.

Condie, K., Pisarevsky, S.A., Korenaga, J., Gardoll, S., 2015. Is the rate of supercontinent assembly changing with time? Precambrian Research 259, 278-289.

Condie, K.C., Kröner, A., 2008. When did plate tectonics begin? Evidence from the geologic record, in: Condie, K.C., Pease, V. (Eds.), When did plate tectonics begin? Geological Society of America special paper 440, pp. 281-294.

Corfu, F., Hanchar, J.M., Hoskin, P.W.O., Kinny, P., D., 2003. Atlas of zircon textures, in: Hanchar, J.M., Hoskin, P.W.O. (Eds.), Zircon. Mineralogical Society of America, pp. 469-500.

Dhuime, B., Hawkesworth, C.J., Cawood, P.A., Storey, C.D., 2012. A Change in the Geodynamics of Continental Growth 3 Billion Years Ago. Science 335, 1334-1336.

Frost, B.R., Frost, C.D., 2008. On charnockites. Gondwana Research 13, 30-44.

Geisler, T., Schaltegger, U., Tomaschek, F., 2007. Re-equilibration of Zircon in Aqueous Fluids and Melts. Elements 3, 43-50.

Gerya, T., 2014. Precambrian geodynamics: Concepts and models. Gondwana Research 25, 442-463.

Gerya, T.V., Stern, R.J., Baes, M., Sobolev, S.V., Whattam, S.A., 2015. Plate tectonics on the Earth triggered by plume-induced subduction initiation. Nature 527, 221-225.

Goodwin A. M., 1991. Precambrian Geology. The Dynamic Evolution of the Continental Crust. xiv 666 pp. London, San Diego, New York, Berkeley, Boston, Sydney, Tokyo, Toronto: Academic Press

Griffin, W.L., Belousova, E.A., O'Neill, C., O'Reilly, S.Y., Malkovets, V., Pearson, N.J., Spetsius, S., Wilde, S.A., 2014. The world turns over: Hadean–Archean crust–mantle evolution. Lithos 189, 2-15.

Griffin, W.L., O''Reilly, S.Y., Abe, N., Aulbach, S., Davies, R.M., Pearson, N.J., Doyle, B.J., Kivi, K., 2003. The origin and evolution of Archean lithospheric mantle. Precambrian Research 127, 19-41.

Grimes, C.B., John, B.E., Cheadle, M.J., Mazdab, F.K., Wooden, J.L., Swapp, S., Schwartz, J.J., 2009. On the occurrence, trace element geochemistry, and crystallisation history of zircon from in situ ocean lithosphere. Contributions to Mineralogy and Petrology 158, 757-783.

Harley, S.L., Kelly, N.M., Möller, A., 2007. Zircon Behaviour and the Thermal Histories of Mountain Chains. Elements 3, 25-30.

Hoskin, P.W.O., Black, L.P., 2000. Metamorphic zircon formation by solid-state recrystallisation of protolith igneous zircon. Journal of Metamorphic Geology 18, 423-439.

Hoskin, P.W.O., Schaltegger, U., 2003. The Composition of Zircon and Igneous and Metamorphic Petrogenesis, in: Hanchar, J.M., Hoskin, P.W.O. (Eds.), Zircon. Mineralogical Society of America, pp. 27-62.

Hyndman, R.D., Currie, C.A., Mazzotti, S.P., 2005. Subduction zone backarcs, mobile belts, and orogenic heat. GSA Today 5, 4-10.

King, S.D., 2005. Archean cratons and mantle dynamics. Earth and Planetary Science Letters 234, 1-14.

Kirkland, C.L., Smithies, R.H., Taylor, R.J.M., Evans, N. and McDonald, B., 2015. Zircon Th/U ratios in magmatic environs. Lithos, 212, pp.397-414.

Kusiak, M.A., Whitehouse, M.J., Wilde, S.A., Nemchin, A.A., Clark, C., 2013. Mobilization of radiogenic Pb in zircon revealed by ion imaging: Implications for early Earth geochronology. Geology 41, 291-294.

Le Maitre R. W. (Editor), Streckeisen A., Zanettin B., Le Bas M. J., Bonin B., Bateman P., Bellieni G., Dudek A., Efremova S., Keller J., Lameyre J., Sabine P.A., Schmid R., Sørensen H., Woolley A.R., 2002. Igneous Rocks: A Classification and Glossary of Terms. Cambridge, UK: Cambridge University Press, 252 p.

Leake, B.E., Woolley, A.R., Arps, C.E.S., Birch, W.D., Gilbert, M.C., Grice, J.D., Hawthorne, F.C., Kato, A., Mandarino, J.A., Maresch, W.V., Nikel, E.H., Rock, N.M.S., Schumacher, J.C., Smith, D.C., Stephenson, N.C.N., Ungaretti, L., Whittaker, E.J.W., Youzhi, G., 1997. Nomenclature of amphiboles: Report of the Subcommittee on Amphiboles of the

International Mineralogical Association, Commission on New Minerals and Mineral Names. . Canadian Mineralogist 35, 219-246.

Lobach-Zhuchenko, S.B., Chekulaev, V.P., Arestova, N.A., Krasnova, A.F., 1979. K-Ar zones of the eastern part of the Baltic Shield and a comparison of them with some structures of the Russian Platform basement, in: Kratz, K.O. (Ed.), Main problems of the Russian Platform Geology. Nauka, Leningrad, pp. 83-93.

Mints, M.V., 2011. 3D model of deep structure of the Early Precambrian crust in the East European Craton and paleogeodynamic implications. Geotectonics 45, 267-290.

Molina, J.F., Moreno, J.A., Castro, A., Rodríguez, C., Fershtater, G.B., 2015. Calcic amphibole thermobarometry in metamorphic and igneous rocks: New calibrations based on plagioclase/amphibole Al-Si partitioning and amphibole/liquid Mg partitioning. Lithos 232, 286-305.

Moyen, J.-F., 2011. The composite Archaean grey gneisses: Petrological significance, and evidence for a non-unique tectonic setting for Archaean crustal growth. Lithos 123, 21-36.

Moyen, J.-F., Laurent, O., 2018. Archaean tectonic systems: A view from igneous rocks. Lithos 302–303, 99-125.

Moyen, J.-F., Martin, H., 2012. Forty years of TTG research. Lithos 148, 312-336.

Muslimov, R.K., Lapinskaya, T.A., 1996. The Crystalline Basement in Tatarstan and Problems of the Presence of Oil and Gas Deposits. Denta, Kazan, p. 488.

Pearce J.A., 1996. Sources and settings of granitic rocks. Episodes 19 (4). 120–125.

Pearce, J.A., Harris, N.W., and Tindle, A.G., 1984.Trace element discrimination diagrams for the tectonic interpretation of granitic rocks, J. Petrol. 25, 956–983.

Pease, V., Percival, J., Smithies, H., Stevens, G., Van Kranendonk, M., 2008. When did plate tectonics begin? Evidence from the orogenic record, in: Condie, K.C.a.P., V. (Ed.), When did plate tectonics begin on planet Earth? Geological Society of America, Boulder, USA, pp. 199-228.

Piazolo, S., Austrheim, H., Whitehouse, M., 2012. Brittle-ductile microfabrics in naturally deformed zircon: Deformation mechanisms and consequences for U-Pb dating. American Mineralogist 97, 1544–1563.

Piazolo, S., La Fontaine, A., Trimby, P., Harley, S., Yang, L., Armstrong, R., Cairney, J.M., 2016. Deformation-induced trace element redistribution in zircon revealed using atom probe tomography. Nature Communications 7, 10490.

Polevaya, N.I., 1978. Catalogue of age determinations of the USSR rocks by isotopic methods. The Russian Platform (the crystalline basement and volcanic-sedimentary cover). The All-Union Geological Institute (VSEGEI), Leningrad, p. 300.

Postnikov, A.V., 2002. The basement of the eastern part of the East European Platform and its influence upon the structure and oil-and-gas bearing of the sedimentary cover, The Faculty of Petroleum Geology and Geophysics. The Gubkin State University of Oil and Gas Moscow, Russia, p. 52.

Postnikov, D.V., 1976. A comparison of data on the absolute age of various rocks from the crystalline basement of the Volgo-uralian province, Problems of Isotope Geology of the Urals and the eastern part of the Russian Platform. Institute of Geology, the USSR Academy of Sciences, Ufa, pp. 14-47.

Rajesh, H.M., 2012. A geochemical perspective on charnockite magmatism in Peninsular India. Geoscience Frontiers 3, 773-788.

Rajesh, H.M., Santosh, M., 2012. Charnockites and charnockites. Geoscience Frontiers 3, 737-744.

Rimša, A., Whitehouse, M.J., Johansson, L., Piazolo, S., 2007. Brittle fracturing and fracture healing of zircon: An integrated cathodoluminescence, EBSD, U-Th-Pb, and REE study. American Mineralogist 92, 1213-1224.

Savko, K.A., Samsonov, A.V., Sal'nikova, E.B., Kotov, A.B., Bazikov, N.S., 2015. HT/LP Metamorphic Zoning in the Eastern Voronezh Crystalline Massif: Age and Parameters of Metamorphism and Its Geodynamic Environment. Petrology (Petrologya) 23, 559-575

Sizova, E., Gerya, T., Stüwe, K., Brown, M., 2015. Generation of felsic crust in the Archean: A geodynamic modeling perspective. Precambrian Research 271, 198-224.

Spruzeniece, L., Piazolo, S., Maynard-Casely, H.E., 2017. Deformation-resembling microstructure created by fluid-mediated dissolution-precipitation reactions. Nature Communications 8.

Taylor SR, McLennan SM. 1985. The continental crust: its composition and evolution. Blackwell, Oxford

Terentiev, R.A., Savko, K.A., Samsonov, A.V., Larionov, A.N., 2014. Geochronology and geochemistry of acid metavolcanites, Losevo Series, Voronezh crystalline massif. Doklady Earth Sciences 454, 136-139.

Terentiev, R.A., Skryabin, V.Y., Santosh, M., 2016. U–Pb zircon geochronology and geochemistry of Paleoproterozoic magmatic suite from East Sarmatian Orogen: Tectonic implications on Columbia supercontinent. Precambrian Research 273, 165-184.

Tretiakova, I. G., Belousova, E. A., Malkovets, V. G., Griffin, W. L., Piazolo, S., Pearson, N. J., O'Reilly S.Y., Nishido, H. (2017). Recurrent magmatic activity on a lithosphere-scale structure: Crystallisation and deformation in kimberlitic zircons. Gondwana Research, 42, 126-132.

Trofimov, V.A., 2006. Deep CMP seismic surveying along the Tatseis-2003 Geotraverse across the Volga-Ural petroliferous province Geotectonics (Geotektonika) 40, 249-262.

Van Kranendonk, M.J., Kirkland, C.L., Cliff, J., 2015. Oxygen isotopes in Pilbara Craton zircons support a global increase in crustal recycling at 3.2Ga. Lithos 228-229, 90-98.

Vervoort, J.D., Patchett, P.J., 1996. Behavior of hafnium and neodymium isotopes in the crust: constraints from Precambrian crustally derived granites. Geochim. Cosmochim. Acta 60 (19), 3717–3733.

Wan Y., Liu D., Dong C., Liu S., Wang S., Yang E., 2011. U–Th–Pb behavior of zircons under high-grade metamorphic conditions: A case study of zircon dating of meta-diorite near Qixia, eastern Shandong. Geoscience Frontiers Volume 2, Issue 2, 137-146

Watson E.B. & Harrison T.M. 2005. Zircon Thermometer Reveals Minimum Melting Conditions on Earliest Earth. Science 308, 841-844.Watson, E.B., Wark, D.A., Thomas, J.B., 2006. Crystallisation thermometers for zircon and rutile. Contributions to Mineralogy and Petrology 151, 413.

Whalen, J.B., Currie, K.L., and Chappell, B.W., 1987. A type granites: geochemical characteristics, discrimination, and petrogenesis. Contrib. Mineral. Petrol., 95, 407–419.

Yakymchuk, C., Kirkland, C. L., & Clark, C. 2018. Th/U ratios in metamorphic zircon. Journal of Metamorphic Geology, 36(6), 715-737.

Table 1. Major and trace-element composition of the Kolyvan rock suite for representative samples

Suite	Granitoids				Kolyvan (Kol) 1: enderbites				
Drilling site	Parf*	PM**	Tarm*	PM**	Kol*	Kol*	Gorb**	Dzerzh	Gorb*
# drillcore	50	12	40	18	81	93	51	89	58
Sample	1	1	3	1	1	15	3	7	1
wt %									
SiO_2	55,28	56,74	62,24	64,02	49,11	49,46	51,53	54,02	61,46
TiO_2	1,07	1,05	0,79	0,06	1,27	1,35	0,9	0,33	0,84
Al_2O_3	16,44	16,02	17,83	19,47	13,59	18,99	19,95	20,18	16,42
FeO tot	9,55	7,71	5,00	2,30	13,22	3,44	7,07	7,33	5,55
MnO	0,14	0,05	0,06	0,04	0,20	0,09	0,05	0,11	0,07
MgO	3,62	2,13	2,11	0,63	5,64	4,36	0,63	3,11	1,71
CaO	7,16	3,94	5,63	3,83	10,58	8,75	8,66	6,34	4,66
Na_2O	3,59	3,62	4,27	5,06	3,31	4,49	5,4	4,68	4,50
K_2O	1,66	4,18	1,27	2,13	0,86	1,33	1,25	0,99	2,49
P_2O_5	0,42	0,56	0,24	0,09	0,11	0,61	0,49	0,37	0,37
Loi	1,07	2,94	0,76	2,2	0,34	1,1	3,95	1,58	0,86
Total	99,66	98,94	99,65	99,85	98,23	94,00	99,88	99,04	98,94
ASI	3,6	1,5	2,5	1,2	7,7	2,0	3,1	5,4	1,7
MALI	-1,9	3,9	-0,09	3,4	-6,4	-1,2	-2,0	-0,67	2,3
Trace elements (ppm)									
Ba	889	4074	897	556	219	1122	1468	540	1332
Co	34,6	15,8	13,5	5,3	40	34	15	44,5	19,0
Cr	44,9	40	26,7	30	126	80	120	100	16,0
Ga	nd	21,9	nd	24,6	16,8	25,4	27,5	31	18,8
Hf	2,99	13,3	4,98	0,9	2,8	7,6	6	0,7	10,5

Nb	7,52	15,6	4,38	1,1	11,0	11,4	4,7	1,1	9,0
Ni	34,6	13,8	13,5	53,8	58,0	59,1	16	33,8	11,0
Pb	18,2	1,5	7,62	3,6	4,0	9,1	2,2	1,7	13
Rb	21,6	59,8	20,8	43,7	16,0	8,6	7,7	9,7	47
Sr	234	554	555	424	151	892	998	541	326
Ta	0,38	0,8	0,19	0,1	0,3	0,3	0,2	0,1	0,41
Th	2,42	9,2	4,5	26,7	1,0	7,2	0,7	1,4	2,1
U	0,44	0,8	0,51	0,5	0,1	0,5	0,2	0,2	0,52
V	142	106	70,7	8	275	169	126	139	87,0
Y	32	36	10	5	24	26	15	13	28
Zr	137	570,1	237	35	67	342	262	21,7	303
La	71	117	56	54	17	124	58	54	54
Ce	156	262,5	99	89,3	38	247,1	123	98,6	130
Pr	19,3	31,42	10,9	8,10	4,25	26,01	15,02	11,06	15,4
Nd	74,6	116,8	39,1	24,2	15,6	89,0	59,3	43,9	64,7
Sm	12,2	18,49	5,18	2,92	3,45	12,08	8,5	6	9,7
Eu	1,41	2,85	1,62	1,47	1,09	2,74	2,38	1,65	1,3
Gd	8,72	12,71	3,71	1,92	3,95	8,35	5,61	3,78	8,3
Tb	1,28	1,62	0,52	0,24	0,66	1,06	0,77	0,53	1,1
Dy	6,99	7,78	2,15	1,13	4,09	5,08	3,23	2,51	4,5
Ho	1,12	1,43	0,67	0,19	0,88	0,95	0,5	0,44	0,78
Er	2,93	3,44	0,81	0,44	2,70	2,42	1,38	1,15	2,4
Tm	0,33	0,53	0,1	0,06	0,36	0,38	0,18	0,14	0,35
Yb	2,32	3	0,65	0,32	2,35	2,12	1,08	0,91	2,4
Lu	0,3	0,45	0,13	0,04	0,34	0,34	0,14	0,14	0,30
(La/Sm)N	3,6	3,9	6,8	11,5	3,1	6,4	4,3	5,8	3,4
(Gd/Yb)N	3,0	3,4	4,6	4,9	1,4	3,2	4,2	3,4	2,8

Eu/Eu*	0,42	0,57	1,13	1,89	0,90	0,83	1,05	1,06	0,46
Nb/Nb*	0,21	0,17	0,10	0,01	0,96	0,14	0,27	0,05	0,31

Table 1. Continued

Suite	Kolyvan (Kol) 1: enderbites			Kolyvan (Kol) 2: charnoenderbites and charnockites				
Drilling site	Kud	Kol*	Kol*	Ras**	Ras**	Ras**	Ras**	Kar**
# drillcore	54	92	92	61	60	61*	73	71
Sample	2	1	1a	2	6	2	2	2
wt %								
SiO_2	64,7	65,62	67,82	67,61	67,76	68,31	68,97	69,96
TiO_2	0,68	0,78	0,61	0,53	0,50	0,53	0,44	0,30
Al_2O_3	16,6	15,40	15,90	14,46	14,88	14,86	14,00	14,29
FeO tot	4,15	4,30	3,10	4,73	3,21	4,03	3,66	2,11
MnO	0,05	0,06	0,04	0,05	0,02	0,02	0,04	0,02
MgO	1,61	1,43	0,89	1,6	0,79	1,2	1,29	0,40
CaO	4,52	3,74	4,27	3,57	1,56	2,19	2,24	3,04
Na_2O	4,19	3,59	4,07	3,75	2,93	3,75	3,65	3,06
K_2O	1,5	3,04	1,86	1,48	6,39	4	3,62	4,10
P_2O_5	0,24	0,30	0,25	0,17	0,32	0,2	0,18	0,09
Loi	1,06	0,81	0,52	1,9	0,8	1,1	1,3	2,2
Total	99,24	99,07	99,33	99,85	99,16	100,19	99,40	99,60
ASI	2,0	1,2	1,3	2,3	0,5	2,1	1,0	0,5
MALI	1,2	2,9	1,7	1,9	7,8	1,7	5,0	4,1
Trace elements (ppm)								
Ba	1198	1707	999	893	4126	2306	2095	3915

Co	41,4	23	21	50	5	47	8	4,1
Cr	10	20	17	90	30	10	20	20,0
Ga	23,4	18	17	21,2	16,6	22,1	17,6	16,7
Hf	6,3	7,5	8,6	1,4	4,9	4,5	4,3	4,1
Nb	9,1	10,0	10	4,5	6,7	3	4,2	3,2
Ni	11,7	10	10	9,7	9,7	9,8	8,6	8,2
Pb	3,3	10,8	9,3	2,3	1,1	3,1	0,9	4,9
Rb	34	56	35	17,6	145,8	90,1	71,8	69,8
Sr	700	404	384	460	511	373	386	615
Ta	0,2	0,36	0,31	0,2	0,2	0,1	0,1	0,3
Th	12,8	2	1,8	0,7	3,6	0,2	0,2	17,6
U	0,3	0,37	0,38	0,1	0,2	0,2	0,1	0,3
V	65	74	48	68	65	43	36	37
Y	17	19	13	5,9	18,3	6,4	5,9	5,7
Zr	263	343	250	55	203	190	180	163
La	99	49	51	47	94	59	57	85
Ce	177	101	102	76,8	185,7	99,1	97,6	154,2
Pr	19	11,7	11,2	8,07	19,69	10,33	9,35	14,36
Nd	71,5	44,2	38,2	29,5	68,0	40,4	31,4	43,5
Sm	9	5,9	5,6	3,7	9,62	5	4,17	4,41
Eu	1,77	1,4	1,4	1,29	1,90	1,2	1,23	1,77
Gd	4,9	5,0	4,2	1,86	6,55	2,4	2,46	2,72
Tb	0,74	0,64	0,53	0,25	0,80	0,33	0,28	0,27
Dy	3,17	2,8	2,6	1,16	3,82	1,1	1,19	1,20
Ho	0,57	0,52	0,47	0,19	0,69	0,24	0,19	0,23
Er	1,44	1,6	1,3	0,42	1,63	0,46	0,49	0,47
`Tm	0,19	0,20	0,14	0,07	0,22	0,07	0,07	0,08

Yb	1,14	1,3	0,9	0,41	1,14	0,38	0,39	0,48
Lu	0,17	0,16	0,13	0,06	0,18	0,07	0,07	0,08
(La/Sm)N	7,1	5,1	5,7	7,9	6,1	7,3	8,5	12,1
(Gd/Yb)N	3,6	3,2	3,7	3,7	4,6	5,1	5,1	4,6
Eu/Eu*	0,81	0,76	0,90	1,50	0,73	1,06	1,17	1,56
Nb/Nb*	0,09	0,37	0,38	0,29	0,13	0,32	0,45	0,03

Drilling sites: Gorb - Gorbatovskaya, Dzerzh - Dzerzhinskaya, Kar - Karagayskaya, Kol - Kolyvanskaya, Kud - Kudinovskaya, Parf - Parfenovskaya, PM - Pod'em-Mikhaylovskaya, Ras - Rassvetskaya, Tarm – Tarmikhinskaya

Analyses* were carried out at the VSEGEI Analytical Centre (St. Petersburg, Russia), and analyses** at the ACME Analytical Laboratories (Vancouver, Canada).

The description of methods is in Appendix 2.

ASI is Al/(Ca-1.67P+Na+K), mol.%

MALI is K2O+Na2O-CaO (wt.%)

Table 2. Sm-Nd isotope data of the dated Kolyvan rocks suite samples

Locality of the drillcore, #well - #sample	Rock	Sm ppm	Nd ppm	($^{147}Sm/^{144}Nd$)	($^{143}Nd/^{144}Nd$)	2□	Zircon age, Ma	ƐNd (T)	T_{DM}
Gorbatovskaya, 51-3	Enderbite	9,67	59,4	0,0984	0,510511	12	3140	-1,7	3464
Tarmikhinskaya, 40-3	Tonalite	5,82	40,6	0,0866	0,510256	8	3130	-2,1	3445
Parfenovskaya, 50-1	Diorite	15,0	87,1	0,1041	0,510643	5	3137	-1,5	3461

Table 3. SIMS/SHRIMP U-Pb analyses of zircon from the granitoids of the Kolyvan rock suite

Spot	% $^{206}Pb_c$	ppm U	ppm Th	$^{232}Th/^{238}U$	ppm $^{206}Pb^*$	(1) $^{206}Pb/^{238}U$ Age		(1) $^{207}Pb/^{206}Pb$ Age		% Dis-cor-dant	(1) $^{207}Pb^*/^{206}Pb^*$	± %	(1) $^{207}Pb^*/^{235}U$	± %	(1) $^{206}Pb^*/^{238}U$	± %	err corr
N-39-1-1 Tarmikhinskaya																	
6,1	0,70	1192	859	0,74	282	1557	± 18	2834.5	± 8.5	82	0.2009	0.52	7.57	1.4	0.2731	1.3	,927
1,1	0,89	1080	559	0,54	272	1644	± 19	2877	± 11	75	0.2062	0.7	8.27	1.5	0.2906	1.3	,883
9,1	0,18	1673	1551	0,96	640	2370	± 25	3050.9	± 5	29	0.2298	0.31	14.08	1.3	0.4443	1.3	,971
4,2	0,34	662	515	0,80	282	2589	± 29	3083.7	± 8.1	19	0.2345	0.51	15.99	1.4	0.4943	1.3	,936
8,1	0,03	346	295	0,88	158	2745	± 30	3080.7	± 9.2	12	0.2342	0.57	17.14	1.5	0.5308	1.3	,920
5,1	0,04	1699	1627	0,99	780	2759	± 29	3080.9	± 4.3	12	0.23418	0.27	17.25	1.3	0.5342	1.3	,978

5,2	0,00	190	165	0,90	91.5	2875	± 33	3101	± 13	8	0.2371	0.8	18.38	1.6	0.5621	1.4	,873
3,2	0,20	238	130	0,56	118	2930	± 33	3130	± 14	7	0.2415	0.88	19.16	1.6	0.5753	1.4	,843
2,2	0,08	147	90	0,63	73.3	2952	± 35	3121	± 13	6	0.2401	0.83	19.23	1.7	0.5809	1.5	,869
4,1	0,05	231	455	2,04	116	2968	± 34	3131	± 14	5	0.2417	0.88	19.49	1.7	0.5848	1.4	,853
3,1	0,62	275	129	0,48	140	2974	± 33	3120	± 13	5	0.24	0.79	19.4	1.6	0.5862	1.4	,869
7,1	0,04	286	108	0,39	145	2984	± 33	3126.9	± 9.8	5	0.241	0.62	19.56	1.5	0.5886	1.4	,911
1,2	0,09	102	163	1,66	51.9	3002	± 38	3130	± 18	4	0.2415	1.1	19.75	1.9	0.5932	1.6	,819
9,2	0,34	91	160	1,81	47.6	3040	± 39	3135	± 18	3	0.2422	1.1	20.12	2	0.6025	1.6	,821
6,2	0,04	100	148	1,53	52.2	3052	± 38	3124	± 16	2	0.2406	1	20.08	1.9	0.6055	1.6	,842

2,1	0,02	198	52	0,27	103	3053	± 34	3127	± 11	2	0.2411	0.69	20.13	1.6	0.6057	1.4	,897

N-39-12 Parfenovskaya

5,1	0,00	281	443	1,63	136	2882	± 32	3086	± 10	7	0.235	0.65	18.26	1.5	0.5637	1.4	,904
9,1	0,00	293	380	1,34	145	2937	± 34	3082	± 10	5	0.2343	0.64	18.65	1.6	0.5771	1.4	,913
3,1	0,00	140	83	0,61	63.7	2735	± 33	3109	± 15	14	0.2384	0.93	17.37	1.8	0.5284	1.5	,849
5,2	0,00	115	136	1,22	56.2	2902	± 36	3122	± 16	8	0.2403	0.99	18.84	1.8	0.5686	1.6	,843
1,2	0,08	103	116	1,17	50.9	2923	± 37	3118	± 17	7	0.2397	1	18.96	1.9	0.5738	1.6	,833
6,1	0,00	107	113	1,10	53.1	2947	± 37	3124	± 17	6	0.2406	1	19.23	1.9	0.5797	1.6	,836
4,1	0,03	231	394	1,76	117	2974	± 34	3127	± 11	5	0.241	0.7	19.48	1.6	0.5862	1.4	,897
2,2	0,03	251	311	1,28	127	2979	± 33	3118	± 13	5	0.2396	0.81	19.41	1.6	0.5873	1.4	,864

2,1	0,07	359	572	1,64	182	2987	± 32	3128.9	± 8.9	5	0.2413	0.56	19.62	1.5	0.5895	1.4	,923
10,1	0,03	358	679	1,96	182	2987	± 32	3125.8	± 8.9	5	0.2409	0.56	19.58	1.5	0.5895	1.4	,924
8,1	0,04	225	251	1,15	115	3008	± 35	3129	± 11	4	0.2413	0.72	19.78	1.6	0.5946	1.5	,899
7,2	0,02	168	172	1,05	87	3035	± 35	3134	± 10	3	0.2421	0.65	20.07	1.6	0.6012	1.4	,911
7.1re	0,06	128	73	0,58	66.4	3035	± 35	3134	± 11	3	0.2422	0.68	20.08	1.6	0.6013	1.5	,905
1,1	0,03	426	827	2,01	221	3041	± 32	3129	± 8.1	3	0.2414	0.51	20.06	1.4	0.6027	1.3	,934
3,2	0,04	81	93	1,19	42.2	3050	± 40	3126	± 18	2	0.2409	1.2	20.09	2	0.605	1.7	,820
7,1	0,07	142	82	0,59	78.2	3183	± 96	3306	± 12	4	0.27	0.74	23.76	3.9	0.638	3.8	,982

Errors are 1-sigma; Pbc and Pb* indicate the common and radiogenic portions, respectively.

Error in Standard calibration was 0.53%(not included in above errors but required when comparing data from different mounts).

(1) Common Pb corrected using measured 204Pb.

.1 - analysis of central part; .2 - analysis of outer rim (except for N39-12_7.1 & 7.2 which both from internal part).

Table 4. SIMS/SHRIMP U-Pb analyses of zircon from the Gorbatovskaya 51 enderbite of the Kolyvan rock suite

Spot	**% $^{206}Pb_c$**	**ppm U**	**ppm Th**	**^{232}Th/^{238}U**	**ppm $^{206}Pb^*$**	**(1) ^{206}Pb/^{238}U Age**		**(1) ^{207}Pb/^{206}Pb Age**		**% Dis-cor-dant**	**(1) $^{207}Pb^*$/$^{206}Pb^*$**	**± %**	**(1) $^{207}Pb^*$/^{235}U**	**± %**	**(1) $^{206}Pb^*$/^{238}U**	**± %**	**err corr**
svt13-12r	0,890	19	20	0,95	5,7	1918	155	1718	134	12,4	0,1174	0,010	4,905	0,57	0,3029	0,02	0,85
svt13-2r	0,225	14	14	1,00	4,7	1814	102	1869	146	-3,2	0,1109	0,006	5,156	0,50	0,3373	0,03	0,85
svt13-3r	-	16	14	1,14	5,7	1915	108	1966	153	-2,8	0,1172	0,007	5,779	0,57	0,3575	0,03	0,85
svt13-14r	-	24	27	0,89	8,7	1996	56	2004	146	-0,1	0,1227	0,004	6,148	0,50	0,3635	0,03	0,85
svt13-6	0,078	121	99	1,22	44,9	2117	130	2048	132	3,4	0,1314	0,010	6,772	0,66	0,3738	0,02	0,85
svt13-8	0,070	61	55	1,11	22,9	2086	46	2064	135	0,9	0,1291	0,003	6,734	0,48	0,3783	0,02	0,85
svt13-2r2	-	37	212	0,17	14,6	2134	110	2149	117	-0,8	0,1327	0,008	7,251	0,64	0,3962	0,02	0,85
svt13-3r2	-	70	195	0,36	30,3	2208	43	2335	128	-5,3	0,1385	0,003	8,325	0,56	0,4359	0,03	0,85
svt13-1r	-	52	205	0,25	23,7	2291	124	2437	130	-6,0	0,1453	0,011	9,210	0,88	0,4597	0,03	0,85
svt13-9	-	52	269	0,19	25,1	2589	16	2556	149	1,4	0,1732	0,002	11,610	0,81	0,4861	0,03	0,85
svt13-7	-	22	193	0,11	10,8	2494	62	2587	135	-3,6	0,1637	0,006	11,140	0,81	0,4937	0,03	0,85
svt13-3c	0,079	65	63	1,03	32,2	2762	113	2611	159	5,9	0,1923	0,013	13,219	1,25	0,4986	0,03	0,85
svt13-13r	-	92	195	0,47	45,8	2751	17	2620	153	4,9	0,1910	0,002	13,210	0,90	0,5017	0,03	0,85

svt13-15c	0,052	135	200	0,68	67,9	2838	18	2657	157	7,4	0,2014	0,002	14,068	0,96	0,5066	0,03	0,85
svt13-1c	-	60	68	0,88	33,1	2937	72	2851	165	3,2	0,2141	0,010	16,386	1,29	0,5550	0,04	0,85
svt13-15r	0,040	71	64	1,11	39,3	3000	20	2861	182	5,1	0,2226	0,003	17,099	1,21	0,5570	0,04	0,85
svt13-16c	0,022	336	434	0,77	193,7	3089	15	2962	171	4,6	0,2353	0,002	18,845	1,27	0,5808	0,04	0,85
svt13-4	-	64	62	1,03	37,2	2839	71	2974	175	-4,5	0,2016	0,009	16,280	1,27	0,5857	0,04	0,85
svt13-14r2	0,014	119	204	0,58	69,3	2996	17	2974	171	0,6	0,2221	0,002	17,967	1,23	0,5868	0,04	0,85
svt13-17c	0,001	236	233	1,01	138,7	3090	14	3007	179	3,0	0,2355	0,002	19,229	1,30	0,5922	0,04	0,85
svt13-5	0,121	99	76	1,30	58,4	2899	41	3013	182	-3,6	0,2091	0,005	17,147	1,19	0,5947	0,04	0,85
svt13-2c	-	68	58	1,17	41,5	2919	41	3094	184	-5,5	0,2117	0,005	17,928	1,25	0,6142	0,04	0,85
svt13-11	0,059	71	71	1,00	43,4	3136	19	3105	189	1,4	0,2424	0,003	20,577	1,45	0,6156	0,04	0,85
svt13-9c	-	82	69	1,19	51,2	3151	20	3150	197	0,2	0,2447	0,003	21,219	1,51	0,6290	0,04	0,85
svt13-10	0,106	90	86	1,05	56,2	3134	22	3151	194	-0,3	0,2421	0,003	20,978	1,50	0,6285	0,04	0,85
svt13-14c	0,008	707	419	1,69	445,2	3139	8	3176	201	-0,9	0,2430	0,001	21,247	1,42	0,6343	0,04	0,85
svt13-12c	0,301	56	72	0,78	37,0	3082	70	3302	215	-6,3	0,2344	0,010	21,509	1,91	0,6656	0,05	0,85

Errors are 1-sigma; Pbc and Pb* indicate the common and radiogenic portions, respectively.

Error in Standard calibration was 0.53%(not included in above errors but required when comparing data from different mounts).

(1) Common Pb corrected using measured 204Pb.

Table 5. LA-ICPMS U-Pb analyses of zircon from the Gorbatovskaya 51 enderbite of the Kolyvan suite

Analysis No.	CONCENTRATIONS (ppm)		ratios								AGES (Ma)								
	Th	U	207Pb/206Pb	± 2σ	207Pb/235U	± 2σ	206Pb/238U	± 2σ	208Pb/232Th	± 2σ	207Pb/206Pb	± 2σ	207Pb/235U	± 2σ	206Pb/238U	± 2σ	208Pb/232Th	± 2σ	Discor-dance (%)
*SVT13-37Rim	33	25	0,1178	0,0075	5 845	0,356	0,3598	0,0129	0,1030	0,0093	1923	116	1953	52	1981	60	1981	170	-0,1
04_97-31Rim	42	50	0,1192	0,0061	5 720	0,286	0,3480	0,0107	0,0932	0,0075	1944	94	1934	44	1925	50	1800	138	1,2
04_97-37Rim	35	32	0,1201	0,0086	5 763	0,393	0,3482	0,0137	0,0882	0,0074	1957	130	1941	60	1926	66	1708	138	1,9
04_97-33Rim	59	86	0,1215	0,0076	5 903	0,357	0,3525	0,0123	0,0856	0,0094	1979	114	1962	52	1946	58	1660	176	1,9
04_97-103Rim	31	32	0,1237	0,0052	6 007	0,250	0,3521	0,0100	0,0912	0,0047	2011	76	1977	36	1945	48	1764	88	3,8
05_73-14Rim	40	44	0,1256	0,0095	5 863	0,402	0,3385	0,0106	0,0966	0,0030	2038	136	1956	60	1879	52	1863	54	9,0
04_97-35Rim	114	143	0,1257	0,0059	5 958	0,272	0,3439	0,0098	0,0935	0,0070	2039	84	1970	40	1905	46	1806	130	7,6
05_73-21Rim	25	22	0,1362	0,0044	7 648	0,245	0,4073	0,0101	0,1134	0,0045	2180	58	2190	28	2202	46	2171	80	-1,2
04_97-105Rim	29	491	0,1435	0,0095	7 800	0,505	0,3956	0,0138	0,0964	0,0135	2270	116	2208	58	2149	64	1860	248	6,6
04_97-39Rim	148	122	0,1561	0,0065	8 095	0,333	0,3763	0,0106	0,0822	0,0048	2414	72	2242	38	2059	50	1596	90	17
05_73-09Rim	71	368	0,1605	0,0050	10 061	0,325	0,4548	0,0110	0,1244	0,0067	2461	54	2440	30	2417	48	2370	120	2,2
04_97-102Rim	44	70	0,1608	0,0059	9 024	0,333	0,4072	0,0110	0,0902	0,0047	2464	64	2340	34	2202	50	1745	86	13
04_97-34Rim	93	225	0,1768	0,0093	10 988	0,569	0,4510	0,0141	0,1107	0,0112	2623	90	2522	48	2400	62	2123	204	10
*SVT13-01Rim	59	92	0,2029	0,0101	12 686	0,527	0,4536	0,0124	0,1235	0,0035	2849	82	2657	40	2411	56	2354	62	7
*SVT13-19Rim	92	111	0,2144	0,0086	14 597	0,591	0,4938	0,0139	0,1335	0,0094	2939	66	2789	38	2587	60	2532	168	10
05_73-05Rim	101	122	0,2157	0,0062	17 147	0,512	0,5767	0,0140	0,1576	0,0070	2948	48	2943	28	2935	58	2958	122	0,6
SVT13-07Rim	138	141	0,2201	0,0086	15 669	0,627	0,5165	0,0146	0,1427	0,0098	2981	64	2857	38	2684	62	2696	174	8
SVT13-38Core	78	69	0,2212	0,0111	16 622	0,814	0,5455	0,0161	0,1369	0,0119	2989	82	2913	46	2807	68	2593	212	-4
SVT13-30Rim	66	76	0,2221	0,0103	15 761	0,723	0,5148	0,0157	0,1459	0,0119	2996	76	2862	44	2677	66	2752	210	30
05_73-102Rim	311	364	0,2230	0,0059	16 818	0,458	0,5470	0,0125	0,1500	0,0060	3003	44	2925	26	2813	52	2824	106	7,8

05_73-15Rim	105	105	0,2248	0,0066	17 759	0,534	0,5731	0,0136	0,1551	0,0072	3015	48	2977	28	2920	56	2914	126	3,9
SVT13-19Core	243	286	0,2251	0,0074	16 757	0,571	0,5400	0,0139	0,1386	0,0076	3018	54	2921	32	2783	58	2623	136	13
05_73-17Core	393	446	0,2255	0,0066	16 931	0,514	0,5445	0,0129	0,1469	0,0071	3021	48	2931	30	2802	54	2771	124	8,9
SVT13-06	110	97	0,2265	0,0062	17 356	0,501	0,5557	0,0135	0,1487	0,0062	3028	44	2955	28	2849	56	2802	108	7
SVT13-03	100	85	0,2285	0,0062	16 894	0,486	0,5364	0,0131	0,1496	0,0060	3041	44	2929	28	2768	54	2818	106	18
05_73-103Rim	226	204	0,2288	0,0076	19 275	0,636	0,6109	0,0141	0,1692	0,0096	3044	54	3056	32	3074	56	3159	166	-1,3
SVT13-07C	277	175	0,2290	0,0077	17 579	0,624	0,5566	0,0151	0,1435	0,0082	3045	56	2967	34	2853	62	2710	146	7
SVT13-37Core	189	121	0,2309	0,0097	19 343	0,809	0,6080	0,0165	0,1515	0,0109	3058	70	3059	40	3062	66	2851	190	15
05_73-16Rim	1016	679	0,2318	0,0092	17 770	0,723	0,5560	0,0152	0,1398	0,0095	3065	64	2977	40	2850	62	2645	170	8,7
05_73-05Core	96	84	0,2322	0,0071	19 426	0,586	0,6068	0,0139	0,1622	0,0078	3067	50	3063	30	3057	56	3038	134	0,4
SVT13-05Core	136	114	0,2339	0,0065	18 390	0,540	0,5702	0,0140	0,1522	0,0065	3079	46	3010	28	2909	58	2864	114	11
SVT13-01C	194	127	0,2349	0,0061	18 483	0,521	0,5708	0,0140	0,1529	0,0059	3085	42	3015	28	2911	58	2877	102	4
05_73-19Rim	136	118	0,2352	0,0077	19 801	0,666	0,6108	0,0155	0,1656	0,0090	3088	54	3082	32	3073	62	3097	156	0,6
05_73-101Rim	97	132	0,2369	0,0061	20 209	0,537	0,6189	0,0142	0,1683	0,0063	3099	42	3101	26	3106	56	3144	108	-0,3
05_73-01Rim	91	143	0,2371	0,0056	19 800	0,477	0,6058	0,0130	0,1689	0,0054	3100	38	3082	24	3053	52	3155	94	1,9
04_97-101Rim	346	384	0,2397	0,0071	20 668	0,621	0,6253	0,0144	0,1761	0,0088	3118	48	3123	30	3131	58	3279	152	7,6

* Rejected analysis

Table 6. LA-ICPMS trace-elements data (ppm) for zircon from the Gorbatovskaya 51 enderbite of the Kolyvan suite

Analysis No.	**P**	**Ti**	**Y**	**Nb**	**La**	**Ce**	**Pr**	**Nd**	**Sm**	**Eu**	**Gd**	**Dy**	**Ho**	**Er**	**Yb**	**Lu**	**Hf**	**Ta**	**Pb**	**Th**	**U**	**Th/U**
SVT13-01Core	152	11,7	733	1,35	0,07	32	0,33	5,0	7,6	2,32	30	80	26	107	176	32	10347	0,34	88	148	104	1,43
SVT13-01Rim	120	9,1	268	1,37	0,02	25	0,06	0,64	1,5	0,36	6,1	23	8,3	39	83	17	12310	0,33	40	41	69	0,59
SVT13-04	172	11	525	1,60	0,02	27	0,13	1,8	3,6	1,04	14	47	16	70	129	24	11331	0,38	54	77	70	1,10
SVT13-05	188	11,5	509	1,62	0,02	32	0,09	1,7	3,0	1,19	14	43	15	64	116	22	12491	0,35	76	104	94	1,11
SVT13-06	196	11,3	564	1,66	0,04	33	0,11	1,5	2,7	0,86	13	43	16	66	121	23	13589	0,34	66	94	86	1,09
SVT13-07Core	222	11,8	1255	1,37	0,11	36	0,52	9,3	12,5	3,40	41	102	33	133	221	39	14154	0,33	98	182	122	1,49
SVT13-19Core	257	14,2	804	3,34	0,05	37	0,11	1,1	1,5	0,44	7,9	33	13	66	170	33	25713	1,36	131	145	188	0,77
SVT13-19Rim	231	11,1	912	1,37	0,07	28	0,12	1,7	2,2	0,67	10	39	14	63	126	24	23951	0,31	46	58	74	0,78

SVT13-30Core	225	19,0	1129	2,96	4,97	82	4,76	31	12,3	5,23	25	63	22	100	232	45	19785	0,92	231	330	506	0,65
SVT13-30Rim	200	13	520	1,52	0,08	26	0,11	1,13	1,66	0,50	7,8	27	10	44	89	17	19481	0,25	36	45	53	0,85
SVT13-37Core	859	8,7	5388	1,28	0,04	36	0,21	2,6	5,5	1,94	29	91	31	130	218	40	58074	0,24	87	138	95	1,45
SVT13-37Rim	1117	16,2	2589	1,40	0,00	25	0,06	1,1	1,8	0,48	8,4	27	10	43	83	16	86325	0,23	9	23	19	1,23
SVT13-38Core	1996	8,8	6040	1,33	0,08	23	0,14	1,0	1,9	0,71	10	33	12	52	97	19	150005	0,82	42	57	54	1,05

Table 7. Lu-Hf isotope data for zircon from the the Gorbatovskaya 51 enderbite of the Kolyvan suite

Analysis No.	176Hf/177Hf	1SE	176Lu/177Hf	176Yb/177Hf	Hfinitial	eHf(T)	± SE	TDM (Ga)	TDM Crustal	U-Pb age	2 s
svt13-01Core	0,280794	0,000011	0,000442	0,022081	0,280769	-4,4	0,4	3,36	3,61	2937	36
svt13-01Rim	0,280929	0,000012	0,000284	0,011799	0,280917	-14,3	0,4	3,17	3,66	2291	62
svt13-02Core	0,280828	0,000012	0,000480	0,024135	0,280801	-3,7	0,4	3,32	3,55	2919	20
svt13-02Rim	0,280938	0,000012	0,000254	0,012124	0,280929	-24,9	0,4	3,16	3,89	1814	51
svt13-03Core	0,280805	0,000012	0,000421	0,019366	0,280783	-8,1	0,4	3,35	3,68	2762	56
svt13-03Rim2	0,280896	0,000012	0,000319	0,014662	0,280883	-17,4	0,4	3,22	3,78	2208	21
svt13-04	0,280796	0,000011	0,000280	0,013547	0,280781	-6,3	0,4	3,35	3,64	2839	35
SVT13-2Core	0,280663	0,000016	0,000377	0,016999	0,280642	-9,4	0,6	3,53	3,88	2919	20
SVT13-2Rim	0,280848	0,000013	0,000227	0,009543	0,280840	-28,0	0,5	3,27	4,07	1814	51
SVT13-37Core	0,280761	0,000011	0,000568	0,025974	0,280728	-3,0	0,4	3,42	3,62	3058	35
SVT13-37Rim	0,280902	0,000009	0,000224	0,009863	0,280894	-23,6	0,3	3,20	3,90	1923	58
SVT13-38Rim	0,280702	0,000010	0,000314	0,013410	0,280684	-6,2	0,3	3,47	3,76	2989	41

Lu–Hf CHUR from Bouvier et al. (2008); Earth and Planetary Science Letters 273 (2008) 48–57, using parameters: 176Lu/177Hf CHUR, today =0.0336 ± 1 and 176Hf/177Hf CHUR today =0.282785 ± 11

Scherer et al., 2001 - 176Lu decay constant (1.865x10-11)

1230

Table 8. O-isotope data for zircon from the Gorbatovskaya 51 enderbite

Analysis No.	**$^{18}O/^{16}O$**	**Rel. err in %**	**$\delta^{18}O$**	**± 2□**
svt13-01Core	0,0020174	0,013	6,07	0,24
svt13-01Rim	0,0020178	0,015	6,28	0,24
svt13-03Core	0,0020176	0,012	6,16	0,24
svt13-03Rim	0,0020176	0,011	6,19	0,25
svt13-04	0,0020173	0,010	6,04	0,27
svt13-2Core	0,0020179	0,012	6,34	0,24
svt13-2Rim	0,0020157	0,011	5,26	0,27
svt13-30Core	0,0020168	0,012	5,77	0,26
svt13-30Rim	0,0020176	0,013	6,19	0,22
svt13-31Core	0,0020178	0,012	6,27	0,24
svt13-31Rim	0,0020178	0,012	6,26	0,24
svt13-32Core	0,0020178	0,011	6,29	0,22
svt13-32Rim	0,0020162	0,013	5,49	0,36
svt13-33Core	0,0020171	0,012	5,94	0,25
svt13-33Rim	0,0020173	0,011	6,02	0,24
svt13-34Core	0,0020173	0,012	6,02	0,23
svt13-34Rim	0,0020175	0,012	6,14	0,29
svt13-35Core	0,0020141	0,012	4,44	0,25
svt13-35Rim	0,0020168	0,012	5,79	0,26
svt13-36	0,0020168	0,016	5,77	0,22
svt13-37Core	0,0020168	0,012	5,80	0,21
svt13-37Rim	0,0020180	0,012	6,38	0,25
svt13-38Core	0,0020161	0,011	5,41	0,28
svt13-38Rim	0,0020173	0,011	6,06	0,31
svt13-39Core	0,0020169	0,011	5,84	0,27
svt13-39Rim	0,0020170	0,012	5,91	0,22